Water Air Soil Pollut (2025) 236:151
https://doi.org/10.1007/s11270-025-07782-w

Mesoporous Silica-Polyethyleneimine Composites as High-Capacity Adsorbents for CO_2 Adsorption: Isotherm and Thermodynamic Analysis

Adife Şeyda Yargıç · Mustafa Şener

Received: 21 November 2024 / Accepted: 19 January 2025 / Published online: 4 February 2025

Abstract In this study, polyethyleneimine-mesoporous silica composite materials were prepared and the effectiveness of the promising sorbents in adsorbing CO_2 was evaluated, along with the impacts of the silica support types (Mesoporous Silica Nanoparticles (*MSN*) and Mobil Composition of Matter No.48 (*MCM-48*)), polyethyleneimine (*PEI*) loading percentages (50 and 70 wt.%), calcination, surface functionalization by alkyl chains (*CTMABr*), and adsorption temperature (75 and 100 °C). The analysis's results revealed that the pores of the sorbents were mostly covered with *PEI* molecules following *PEI*-functionalization, and the specific surface area and pore volume were also reduced with rising amine content. The highest CO_2 adsorption capacities were achieved for *UC-MCM-48–50* and *UC-MSN–50* at 2.26 mmol/g and 3.31 mmol/g, respectively. The CO_2 uptake capacities of *CC-MSN–50* and *CC-MCM-48–50*, composed by dispersing *CTMABr* surfactant with the calcined materials before incorporating *PEI*, were remarkably similar to those of non-surfactant functionalized adsorbents. When the temperature's influence on CO_2 adsorption capacity was evaluated, the maximum holding capability adsorbent *UC-MSN–50* had a slight increase in adsorption capacity (~3.6%), whereas *UC-MCM-48–50* had a considerable drop (~23.9%) as the temperature elevated to 100 °C. Besides, Langmuir, Freundlich, Dubinin-Radushkevich, and Temkin isotherms were used to model pure CO_2 adsorption data, and a thermodynamic study was applied. In conclusion, a low-cost and more beneficial approach, which included less *PEI* handling and eliminating the calcination step, was implemented to enhance the CO_2 sorption capacity of composites of *PEI* with the long alkyl chain template *MCM-48* or *MSN* silica support materials.

Keywords Calcination · CO_2 · Gas adsorption · MCM-48 · MSN · Polyethyleneimine

A. Ş. Yargıç (✉) · M. Şener
Chemical Engineering Department, Engineering Faculty, Gulumbe Campus, Bilecik Seyh Edebali University, 11100 Bilecik, Turkey
e-mail: seyda.guler@bilecik.edu.tr; aseydaguler@gmail.com

1 Introduction

The Intergovernmental Panel on Climate Change (*IPCC*) notified that the increase in global warming and the change of the climate are caused by rising levels of inordinate greenhouse gases (*GHGs*) such as carbon dioxide (CO_2), chlorofluorocarbons (*CFCs*), methane (CH_4), nitrous oxide (N_2O), and sulfur hexafluoride (SF_6) in the atmosphere (Al-Ghussain 2019). As a result of the human activities carried out after the Industrial Revolution, there has been a serious increase in atmospheric CO_2 concentration due to deforestation in broad areas and the enhancement of dependence on the burning of fossil fuels. Climate scientists emphasized that more than 30 billion tons of CO_2, which primarily influences global climate change, are anthropogenically released into

the atmosphere annually (Friedlingstein et al., 2010). The CO_2 concentration in the atmosphere reached 400 ppm for the first time in 2015 due to the exponential increase in emissions (Lou et al., 2020). The increase in global temperature between 1951–1980 was determined as 0.8 °C (Sanz-Pérez et al., 2018). The temperature rise was targeted to be limited to 1.5 °C and 2 °C over the levels before industrialization with the Paris Agreement signed in 2015. The rising temperature trend has been classified as endangered in line with actual tendencies in emissions, planned infrastructure, and national policy commitments (Lamb et al., 2021).

Nowadays, in line with the increasing global awareness of CO_2 emissions, preventive and remedial methods come to the fore within the scope of efforts to balance the atmospheric CO_2 concentration and reduce environmental impact (Yan et al., 2011). In this context, it has been emphasized that it is necessary to focus on increasing energy efficiency, using new non-carbon energy sources instead of fossil fuels, and studies on CO_2 capture and storage/utilization applications. Implementing various technologies that remove CO_2 from other exhaust gases leaving a facility, such as the carbon capture technology associated with utilization or sequestration, is an effective way of reducing CO_2 from emissions sources (as well as power plants or industrial facilities). In this regard, CO_2 is trapped before it reaches the environment and either permanently stored underground or added to certain products like concrete or chemicals. Both pre-combustion and post-combustion operations participate in lowering the carbon intensity of power generation and CO_2 capture processes. Whereas pre-combustion relies on designing less carbon-intensive combustion techniques, post-combustion carbon capture aims to extract CO_2 from the exhaust gas streams. The integrated gasification combined cycle (IGCC) and oxyfuel combustion, which employs pure oxygen as fuel, are examples of pre-combustion systems. According to the latest techno-economic reports, energy-intensive CO_2 capture systems must be developed to drastically lower electrical costs and improve combustion efficiency (Nwabueze & Leggett, 2024). The approach developed on the utilization of CO_2 as an alternative to CO_2 storage is aimed at achieving CO_2 conversion to produce compounds such as fuel or synthetic intermediates for pharmaceuticals. Within the CO_2 capture and separation approaches for the control of CO_2 emission, techniques such as membrane separation, solid adsorption, as well as the liquid phase amine scrubbing process, which is the most widely used on an industrial scale due to its high selectivity, are applied (Guo et al., 2017). The different CO_2 capture technologies currently involved in industry and academia are classified in Fig. 1 (Nwabueze & Leggett, 2024). It is known that the absorption process with aqueous amine solutions has disadvantages such as high energy consumption, equipment corrosion, low absorption/desorption ratio, and the amine solution degradation or loss (Sanz-Pérez et al., 2018). Although there is a lack of need for regeneration energy and no residual flows during the usage of the membrane separation, the system should be designed as multi-stage or recycled since membrane separation is restricted to the low separation capacity (Guo et al., 2017).

The following equations indicate the CO_2 chemisorption mechanism related to the interaction among amine groups with CO_2 that generates carbamate under an anhydrous environment. Initially, an amine group attacks CO_2 nucleophilically to generate the zwitterion intermediate such as $RNH_2^+COO^-$ for a primary amine of RNH_2. Meanwhile, the second amine group deprotonates the zwitterion, leading to carbamate formation (Chang et al., 2009; Zeleňák et al., 2008).

$$\text{Step 1}: \ RNH_2 + CO_2 \rightarrow RNH_2{}^+COO^- \tag{1}$$

$$\text{Step 2}: \ RNH_2 + COO^- + RNH_2 \rightarrow RNHCOO^- + RNH_3{}^+ \tag{2}$$

$$\text{Overall reaction}: CO_2 + 2R - NH_2 \rightarrow RNH_3{}^+ + R - NHCOO^- \tag{3}$$

In recent years, interest in applications related to the adsorption process, in which solid-supported amines are used instead of the liquid amine absorption process, has increased. This is because the disadvantages encountered in the absorption process are prominently overcome by the adsorption process. It has been reported that vessel corrosion, solvent loss due to evaporation, and energy consumption are reduced; however, a high adsorption/desorption rate is achieved, and high efficiency and selectivity are provided for CO_2 in gas mixtures when using solid adsorbents modified by amine-loading (Lou et al., 2020).

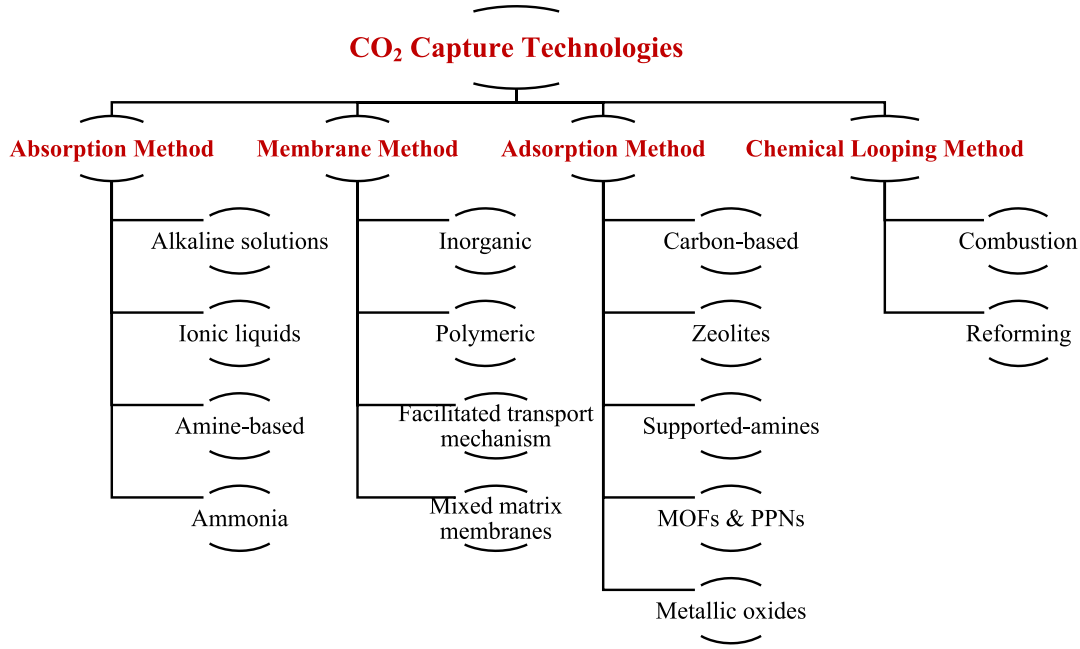

Fig. 1 CO_2 capture strategies applied in both the scientific and industrial sectors

Various adsorbents have been generated for CO_2 uptake comprising porous silica materials (*HPS*, *KIT-6*, *MCM-36*, *MCF*, *MCM-41*, *MCM-48*, *OMS*, *SBA-12*, *SBA-15*, *SBA-16*, etc.) (Fernández-Miranda et al., 2017; Jang et al., 2009; Kishor & Ghoshal, 2017; Liu et al., 2010; Niu et al., 2016; Vilarrasa-García et al., 2014; Wei et al., 2009; Zeleňák et al., 2008; Zhang et al., 2016), porous carbon (Chai et al., 2016; Gholidoust et al., 2017), zeolites (*4A*, *13X*, *ZSM-5*, etc.) (Liu et al., 2017a), *MOFs* (Liao et al., 2016), and porous polymers (Liu et al., 2017b; Mane et al., 2018). The limited selectivity of solid porous materials against CO_2 is a problem. Therefore, studies have focused on adsorbent preparation with high adsorption capacity and selectivity, which are functionalized with organic molecules containing amino groups. The preparation of amine-based silica adsorbents mainly involves one of two methods: either grafting, in which the CO_2-active amino groups are chemically bonded to the silica support using linker silanes, or wet impregnation, in which polymeric amines (polyethyleneimine (*PEI*), tetraethylene-pentamine (*TEPA*), or diethanolamine (*DEA*)) are physically loaded onto the porous substrate surface. The impregnation approach has been utilized more commonly than amine grafting due to its ease of use, reduced price, and capacity to insert substantially more amines than amine grafting to allow more excellent adsorption capabilities. These amine-supported systems have enhanced CO_2 capture capability over bulk amines because the amine molecules are distributed throughout the mesoporous support material's pores (Liu et al., 2019).

The *MCM-48* silica material from the M41S family, which has a 3-D channel system, excellent thermal stability up to 750 °C, narrow pore size distribution, a high specific pore volume, and specific surface area, can be prepared in a variety of approaches (Schumacher et al., 2000). The three-dimensional open-porous *MCM-48* enhances the interaction quantities between catalysts and reagents, which leads to increased activity and resistance to pore blockage. *MCM-48* is effective in applications such as adsorption, catalysis, chromatography, and gas separation (do Nascimento et al., 2016). Mesoporous silica nanoparticles (*MSN*) with stable and expanded mesopores produced by sol–gel and hydrothermal synthesis methods. *MSNs* are renowned for possessing excellent characteristics like uniformly shaped pores with well-defined dimensions. In addition, altering the template molecule's length can modify the pore size of *MSNs*. The surfactants, silica sources, or reaction

parameters, such as temperature, aging period, the mole fraction of reactants, and medium pH, can all be varied to produce an entirely novel mesoporous system (Rameli et al., 2018). Mesoporous inorganic materials are utilized in several disciplines, including catalysis, separation, optics, energy generation and storage, biomedicine, agriculture, and semiconductor nanostructures because of their ordered structures, high surface areas, pore volumes, adjustable size, pore size distribution, compositions, and surface chemistry (Li et al., 2022). Mukherjee and Samanta (2022) impregnated different ratios of benzylamine (*BZA*), monoethanolamine (*MEA*), and aminoethylethanolamine (*AEEA*) onto *MCM-48* to increase the adsorption capacity of CO_2, which were summarized as *MCM-48* (0.637 mmol/g) < *40%BZA-MCM-48* (0.94 mmol/g) < *50%MEA-MCM-48* (1.67 mmol/g) < *30%AEEA-MCM-48* (3.33 mmol/g). In another study, mesoporous *SBA-15* and *MCM-48* silica materials modified with cyclic amines (morpholine and 1-methylpiperazine) demonstrating high CO_2 adsorption potential within 2 and 4.4 mmol/g were prepared (Ravutsov et al., 2021). Qian et al. (2019) confirmed that uncalcined *MCM-48* samples (*MCM-48-W*) functionalized with *PEI* whose pores were coated with cetyltrimethylammonium bromide (*CTMABr*) were more effective CO_2 sorbents than traditional calcined MCM-48 impregnated with *PEI*. The presence of long-alkyl chains could have enhanced the distribution of loaded *PEI* particles, as evidenced by the *MCM-48-W* loaded with 40 wt.% *PEI* demonstrating 2.59 mmol/g of CO_2 adsorption capacity (6.9 mmol-CO_2/g-*PEI*). Several mesoporous silica adsorbents (*MCM-41*, *MCM-48*, *SBA-15*, *SBA-16*, and *KIT-6*) were prepared by Son et al. (2008) and impregnated with 50% *PEI* by weight. The materials' CO_2 sorption abilities changed in the following sequence: *KIT-6* > *SBA-16* ≈ *SBA-15* > *MCM-48* > *MCM-41*. These capacities were all significantly higher than those of pure *PEI* (79 mg-CO_2/g-adsorbent). 119 mg-CO_2/g-adsorbent was the value of the 50% *PEI-MCM-48*'s CO_2 sorption capacity.

Based on the increasing interest in the literature regarding the research of mesoporous materials doped with amine species, this study intended to synthesize silica-based materials impregnated with *PEI* at different weight ratios to improve the CO_2 adsorption capacity, as well as to characterize and clarify their structures using a variety of techniques (XRD, SEM, N_2 sorption, and FT-IR). In this context, two different silica-support materials (*MSN* and *MCM-48*) were used both as-synthesized without calcination and as calcined, and polyethyleneimine was impregnated with 50% and 70% by weight to improve the CO_2 adsorbing ability of the support materials. In addition, 50 wt.% *PEI* was impregnated at the ideal loading ratio after the calcined samples were modified with *CTMABr*. The CO_2 sorption measurement was conducted at atmospheric pressure and 75 °C, and the experiments were then repeated at 100 °C to examine the effect of adsorption temperature for optimum adsorbents. Adsorption experimental data were used to evaluate thermodynamic characteristics and fit the Langmuir, Freundlich, Dubinin-Radushkevich, and Temkin isotherm models.

2 Materials and Methods

2.1 MCM-48 Synthesis Procedure

A gel with a molar composition of *1.0 TEOS: 0.48 NaOH: 0.4 CTMABr: 55* H_2O was prepared to obtain *MCM-48* in a basic medium with the traditional hydrothermal synthesis method (HTS) (Li et al., 2006). Accordingly, *CTMABr* (98%, Alfa Aesar) was completely dissolved at 30 °C using distilled water, *NaOH* (≥98%, Iso Lab) and *TEOS* (98%, Acros Organics) were incorporated in the solution, respectively, and the reaction mixture was agitated for 90 min. After the reaction mixture was transferred to a Teflon bottle, hydrothermal synthesis was carried out for 3 days in an oven at 120 °C. The support material was separated from the synthesis medium using a vacuum filtration system, rinsed with distilled water until pH neutral, and air-dried at room temperature. As-prepared *MCM-48* was coded as *"UC-MCM-48"*, which was then heated to 550 °C with a heating rate of 1 °C/min and calcined for 6 h to prepare the calcined material with the code "*C-MCM-48*".

2.2 MSN Synthesis Procedure

Mesoporous silica nanoparticle (*MSN*) was synthesized by sol–gel method following the recipe suggested by Vazquez et al. (2017), with a molar composition of *1.0 TEOS: 20 EtOH: 1200* H_2O*: 10.4* NH_3*.* H_2O*: 0.3 CTMABr*. A silica solution was prepared

by mixing ethanol (≥98%, Honeywell), distilled water, and ammonia solution (25%, Carlo Erba), then *CTMABr* (98%, Alfa Aesar) was incorporated, and *TEOS* (98%, Acros Organics) was added dropwise. After the synthesis solution was mixed at room temperature for 2 h, the precipitate was removed from the reaction mixture by filtration, rinsed with distilled water until pH neutral, and air-dried at room temperature. Similarly, the as-prepared *MSN* was coded as *"UC-MSN"*, which was then heated to 550 °C with a heating rate of 1 °C/min and calcined for 6 h to prepare the calcined material with the code "*C-MSN*".

2.3 CTMABr-Functionalized CC-MCM-48 and CC-MSN

The calcined silica materials were impregnated with 40% by weight surfactant to form *CC-MCM-48*- and *CC-MSN*-coded materials (Yue et al., 2006). In this context, calcined silica particles were added to *CTMABr* after it had been dissolved in methanol, mixed for 6 h, and finally dried in an oven at 80 °C for 12 h.

2.4 Preparation of PEI-Impregnated Adsorbents

Polyethyleneimine (*PEI*, branched, M.W. 1200, 99%, Alfa Aesar) was loaded at two different impregnation ratios (50% and 70% by weight) to prepare amine-functionalized silica materials, which were known to be accomplished in CO_2 capture. According to the desired amine additive ratio, *PEI* was weighed and dissolved in methanol, mixed with support material, and stirred for 6 h. *PEI*-impregnated silica-based adsorbents were prepared by drying in an oven at 80 °C for 12 h (Yan et al., 2011) and coded as *"S-x"* where *"S"* was the type of support material (*UC-MCM-48, C-MCM-48, UC-MSN, C-MSN, CC-MCM-48* or *CC-MSN*) and *"x"* was denoted as polyethyleneimine loading ratio of 50% or 70% by weight.

2.5 Characterization of Adsorbents

Surface morphologies (particle sizes, shapes, and distributions) of adsorbents were determined by scanning electron microscopy (Zeiss Supra VP 40) with platinum sputter-coated (Quorum Q 150 R ES DC Sputter), total pore volumes (V_{total}), BET surface areas (S_{BET}), and pore size distributions were clarified by Micromeritics TriStar II 3020 instrument via N_2 sorption at 77 K. Fourier transform infrared (FT-IR, Agilent Cary 630) spectrums were taken in the wavenumber range of 4000–400 cm^{-1} to define the functional groups in the structure of the materials, and the crystalline structures were analyzed in PANalytical X'Pert Pro Materials Research Diffractometer using CuKα radiation (λ = 0.15406 nm, in the range of 0–10° 2θ). The CO_2 adsorption capacities of silica-based materials were determined based on their CO_2 isotherms from Micromeritics ASAP 2020 analyzer at 75 and 100 °C. Before the experiments, the materials were outgassed at 100 °C for 3 h.

2.6 CO_2 Adsorption Isotherm Modeling and Thermodynamics

Recognition of the interactions between solid adsorbent and adsorbate molecules is facilitated more easily by the gas–solid adsorption isotherm analysis. In certain situations, adsorption isotherm analysis can be beneficial to determine the equilibrium adsorption capacity as well as to comprehend the adsorption performance and mechanism of CO_2 molecules on porous sorbents. The most fundamental theoretical model for describing monolayer adsorption on a homogeneous adsorbent surface with similar adsorption sites is the Langmuir isotherm. Each adsorption site is capable of adsorbing one molecule at a time due to monolayer adsorption, and the adsorbed molecules do not interact with other molecules (Mamaghani et al., 2024). The Langmuir model assumes that the initial layer of adsorbed molecules has stronger adsorption energy and that subsequent adsorbed layers need a higher pressure (Vargas et al., 2012). The affinity between molecules of the adsorbent and adsorbate is expressed by the Langmuir isotherm constant, k_L. Maximum surface coverage and a higher affinity between the adsorbent and adsorbate molecules are indicated by a greater k_L value. The Freundlich isotherm clarifies a non-ideal and reversible adsorption process (Fatima et al., 2023), and is appropriate for multi-layered adsorption on heterogeneous surfaces (Tiwari et al., 2017). Furthermore, the adsorption energy rose exponentially as surface coverage increased due to fewer active sites (El-Desouky et al., 2021). The Freundlich coefficient (n) specifies whether the adsorption is physical ($n > 1$) or chemical ($n < 1$). The Freundlich constant of n

also defines favorable adsorption as $0 < 1/n < 1$; irreversible adsorption as $1/n = 1$; unfavorable adsorption as $1/n > 1$; and $1/n$ close to zero also means heterogeneous adsorption (Mamaghani et al., 2024; Michalkiewicz et al., 2014; Singh & Kumar, 2018). The Dubinin-Radushkevich (D-R) model, in contrast to the Langmuir and Freundlich isotherm models, is a semi-empirical equation in which the pore-filling mechanism models the adsorption. The model implies that adsorption has a multilayered structure that includes Van der Waal's forces and can be applied to physical adsorption processes (El-Desouky et al., 2021). The temperature dependence of the Dubinin-Radushkevich isotherm is one of its distinctive characteristics. The model is typically used to explain the adsorption mechanism onto a heterogeneous surface with a Gaussian energy distribution (Chegeni et al., 2022). The Temkin isotherm model addresses the impacts of indirect adsorbent-adsorbate interactions on the adsorption mechanism. The adsorption is distinguished by a consistent distribution of binding energies up to a certain maximum binding energy (Garnier et al., 2011). The Dubinin Radushkevich and Temkin isotherms additionally contain beneficial details regarding the energy parameters, specifically mean free energy of adsorption and heat of adsorption (Rashidi et al., 2016). The energy parameter E, found in D-R isotherms, represents the binding energy, which defines the type of interaction between the sorbent and CO_2 molecules and also provides information on the adsorption reaction's mechanism. Adsorption is controlled by chemical adsorption if $E > 16$ kJ/mol, driven by an ion-exchange mechanism if $8 < E < 16$ kJ/mol, and influenced by physical forces when $E < 8$ kJ/mol (Fernandez et al., 2022). The adsorption heat (b_T) of all layer molecules in Temkin isotherms is likewise assumed to decrease linearly as surface coverage increases (Chegeni et al., 2022). The Langmuir, Freundlich, Dubinin-Radushkevich, and Temkin models were chosen within the current theoretical adsorption models to fit the experimental data of adsorbed volumes vs. equilibrium pressures in CO_2 adsorption. An overview of these isotherm models' linearized equations is provided in Table 1. The correlation coefficient (R^2), which ranged between 0 and 1, was used to assess the validity of these models; a value nearer unity indicated the most suitable fit to the related isotherm model.

The Gibbs free energy change (ΔG°, J/mol), an adsorption thermodynamic parameter, was determined by Eq. (11) and revealed the process' spontaneity. A greater negative value of ΔG° characterizes more favorable energetically adsorption (Tiwari et al.,

Table 1 The mathematical expressions of linearized isotherm models

Isotherm model	Linear equations	Eq	Plots and terms
Langmuir	$P_e/q_e = \left[1/\left(k_L q_m\right)\right] + P_e/q_m$	(4)	P_e/q_e vs. P_e P_e: The equilibrium pressure of the adsorbate (kPa) q_e: The adsorption capacity (mmol/g) q_m: The maximum adsorption capacity (mmol/g) k_L: The Langmuir isotherm constant (1/kPa)
Freundlich	$logq_e = logk_F + (1/n)logP_e$	(5)	$logq_e$ vs. $logP_e$ k_F: The Freundlich isotherm constant (mmol/(g.kPa$^{1/n}$)) n: The heterogeneity factor
Dubinin-Radushkevich	$lnq_e = lnq_m - k_{DR}\varepsilon^2$ $\varepsilon = RTln(1 + 1/P_e)$ $E = 1/\sqrt{2k_{DR}}$	(6) (7) (8)	lnq_e vs. ε^2 k_{DR}: The Dubinin-Radushkevich isotherm constant (mmol^2/kJ^2) ε: An isotherm parameter of the Polanyi potential (kJ/mmol) R: The gas constant (kJ/mmol.K) T: The absolute temperature (K) E: The mean free energy of adsorption (kJ/mmol)
Temkin	$q_e = Blnk_T + BlnP_e$ $B = RT/b_t$	(9) (10)	q_e vs. lnP_e k_T: The Temkin isotherm constant (mmol/g.kPa) B: The temperature-dependent heat of adsorption (J/mol) R: The gas constant (J/mol.K) T: The absolute temperature (K) b_t: The Temkin constant related to the heat of adsorption (J/mol)

2017). Besides, van't Hoff's formulation in Eq. (12) was applied to find the enthalpy change (ΔH°, J/mol) and the entropy change (ΔS°, J/mol.K) from the slope and intercept by plotting $ln(k_L)$ versus inverse temperature ($1/T$), respectively (Rashidi et al., 2016).

$$\Delta G^{\circ} = -RTln(k_L) \tag{11}$$

$$ln\left(k_L\right) = -(\Delta H^{\circ}/RT) + (\Delta S^{\circ}/R) \tag{12}$$

where k_L is the equilibrium constant (1/kPa) derived from the Langmuir isotherm fit, R is the universal gas constant (8.314 J/mol.K), and T is the absolute temperature (K).

3 Results and Discussion

This section outlined characterization results and CO_2 sorption performances to clarify the effect of silica support material type, calcination state, surfactant incorporation, and amine loading ratio on adsorbent properties.

3.1 SEM Analysis

The morphological structures of adsorbents prepared by using *MCM-48* and *MSN* as silica support were examined via SEM images (Figs. 2 and 3). According to the SEM images of *MSN*-based adsorbents presented in Fig. 2, it was determined that the *UC-MSN* had a rod-like structure with varying lengths in the range of 210–450 nm, and the structure was preserved after the calcination process. It is well known that the textural morphology of *MSN* is influenced by the water and surfactant concentrations employed in the synthesis since the precursor formulation affects the mechanisms governing micelle formation and *CTMABr* arrangement. The silica particles grow longer and expand by the micelle arrangement by increasing the water content. The *TEOS* hydrolysis is reduced, and the formation of the mesoporous silica particle in the direction perpendicular to the pore-alignment is promoted by the solution dilution, which affects the arrangement of the surfactant micelles and generates aggregates that enclose the silica precursor (Vazquez et al., 2017). According to the SEM images (Fig. 3), *UC-MCM-48* consisted of agglomerated spherical particles (Fig. 3a), whereas *C-MCM-48* formed after removing the surfactant from the structure by calcination (Fig. 3d) had smaller and more uniformly shaped spherical morphology compared to *UC-MCM-48* and had different sized particles. After the amine group was impregnated into the support structure, it was revealed that the surface of both non-calcined and calcined particles was covered by *PEI*, which had an adhesive nature.

3.2 XRD Analysis

The x-ray diffraction method was applied to get information about the crystal structures (amorphous, crystalline, or semi-crystalline) of porous materials. X-ray diffraction patterns of *MSN*- and *MCM-48*-based adsorbents were given in Figs. 4 and 5. The characteristic peaks of *MCM-48* and *MSN* silica materials with the highest intensity belong to (2 1 1) and (1 0 0) reflections, respectively (Pirouzmand et al., 2013). The ordered pore structure of the mesoporous silica nanoparticle was supported by the characteristic peak (1 0 0) observed around $2\theta = 2.3°$ in XRD patterns and confirming the hexagonal structure. In the low-angle XRD patterns, weak diffraction peaks around 4° and 4.5° indicated (1 1 0) and (2 0 0) planes, respectively (Alsyouri et al., 2013). Denoting that *MSN* consisted of a long-range ordered hexagonal-phase pore structure was the fact that the three crystal planes' diffraction peaks were compatible with those of the typical mesoporous silica peaks reported for *MCM-41* (Xu et al., 2020). The presence of peaks belonging to (1 0 0), (1 1 0), and (2 0 0) planes confirmed the existence of a two-dimensional hexagonal (*p6mm*) structure with a d_{100} interval of approximately 3.9 nm (Sazegar et al., 2017). Besides, the weak diffraction peak of the (2 2 0) plane was observed around $2\theta = 6°$ (Das et al., 2004). While it was known that the mesostructure order diminished as the diffraction peak widened, the narrow peak at $2\theta = 2.3°$ demonstrated that the pore size and arrangement were identical. A weak regular or irregular mesoscopic structure was indicated by the lack of a clearly defined diffraction peak in XRD diffraction patterns (Han et al., 2013). In this case, the increase in peak intensity revealed the presence of highly ordered and crystalline structures in the materials. It was established through x-ray diffraction patterns that the amine group's

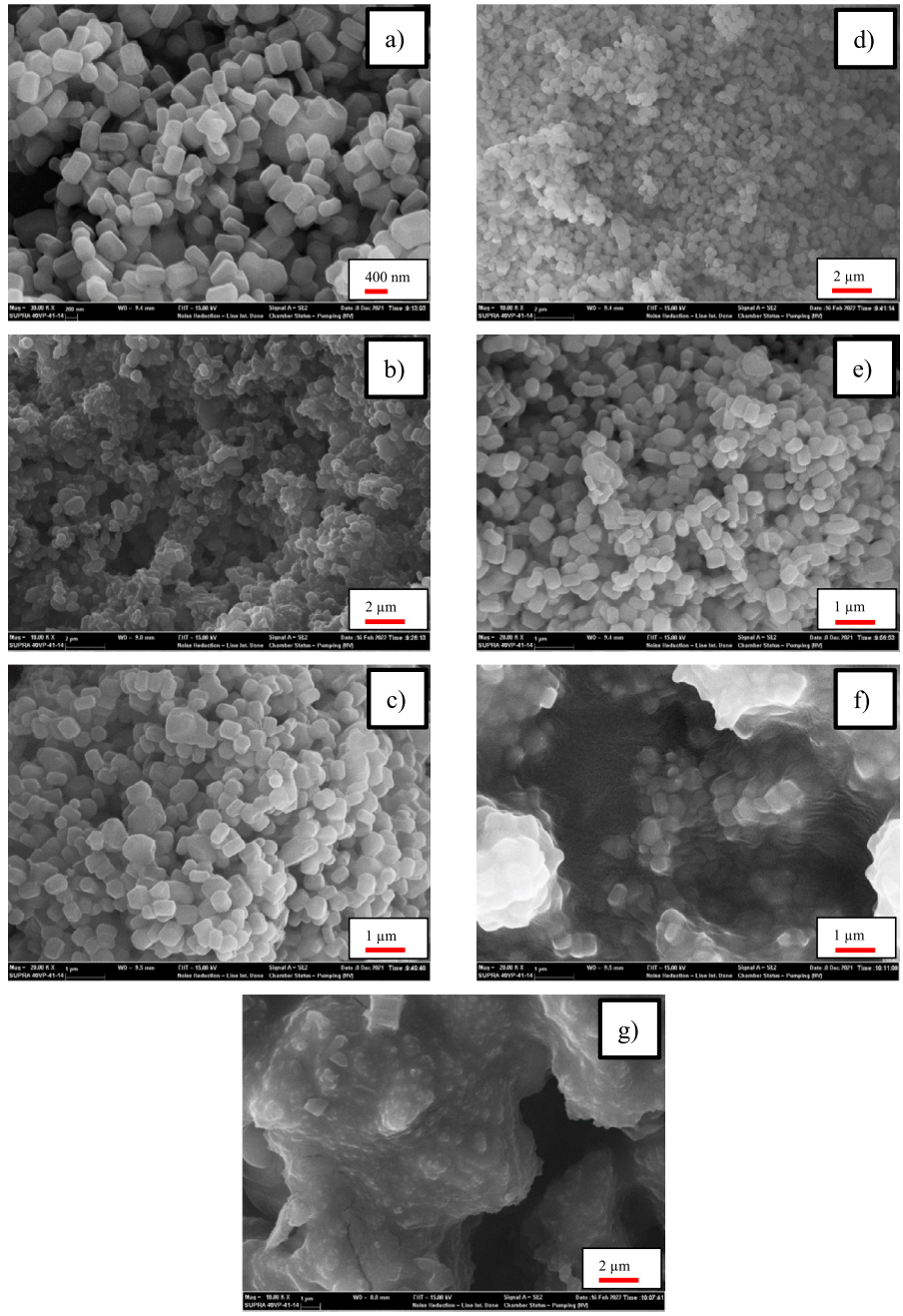

Fig. 2 SEM images of *MSN*-based adsorbents at 10.00 and 20.00 kX magnification (**a**) *UC-MSN*, (**b**) *UC-MSN–50*, (**c**) *UC-MSN–70*, (**d**) *C-MSN*, (**e**) *C-MSN–50*, (**f**) *C-MSN–70*, and **g**) *CC-MSN–50*

impregnation into the support structure caused a decrease in the intensity of the (1 0 0) peak and a change in the peak position. The reduction in x-ray intensity should be attributed to the combined influence of increased disorder and a significant phase-distortion phenomenon associated with scattering *PEI* particles starting to settle into the pore spaces in the support material (Das et al., 2016).

Peaks corresponded to the cubic mesophase *MCM-48*'s *Ia3d* space group (comprising planes (2 1 1), (2 2 0), (4 2 0), and (3 3 2)) were detected in *MCM-48* structures (Wang et al., 2012). *MCM-48* materials were prepared in a highly ordered structure, according to the XRD patterns seen in Fig. 5. Moreover, it was noted that when *PEI* concentration increased, the principal diffraction peak (2 1 1) shifted to higher 2θ values.

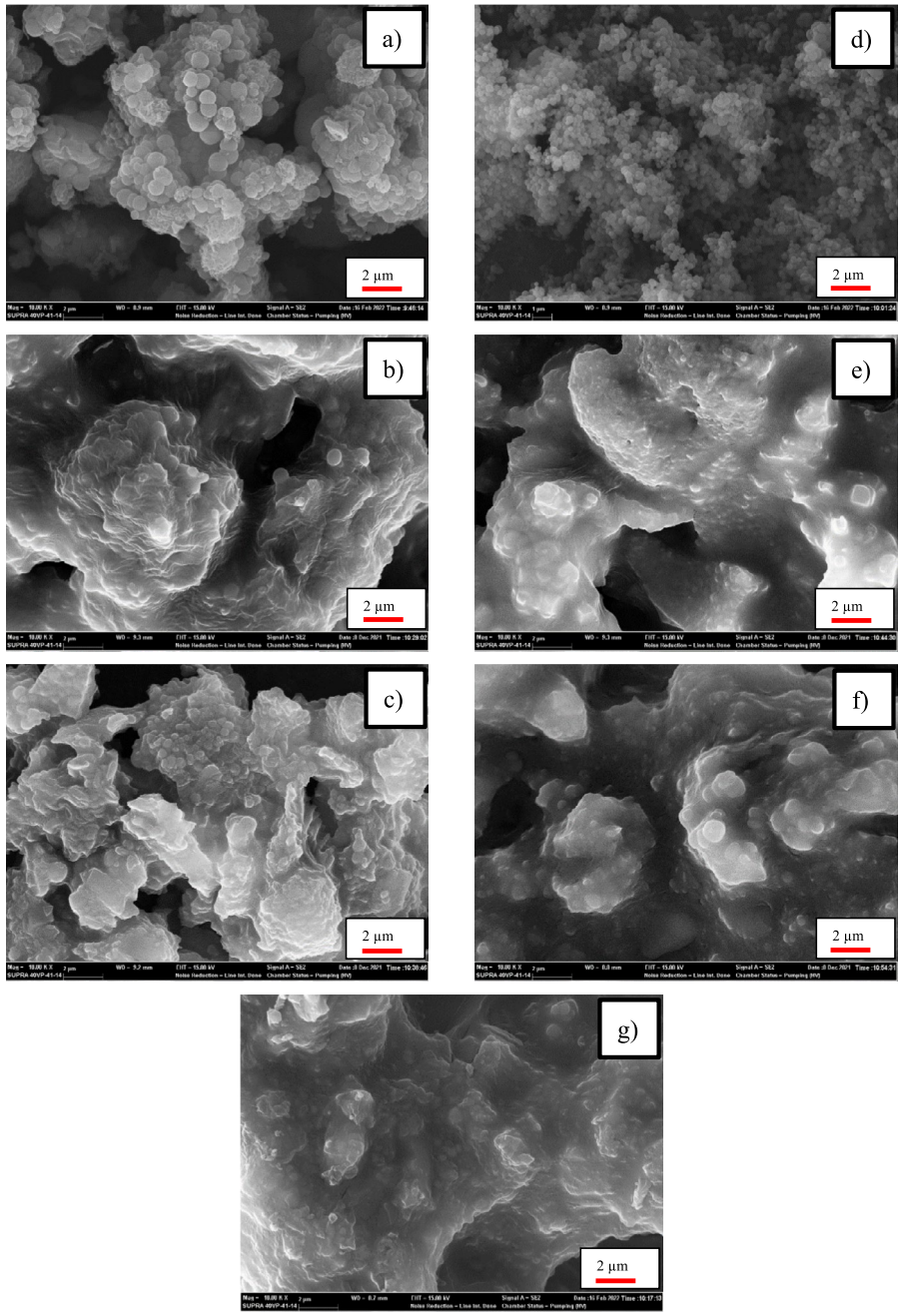

Fig. 3 SEM images of *MCM-48*-based adsorbents at 10.00 kX magnification (**a**) *UC-MCM-48,* (**b**) *UC-MCM-48–50,* (**c**) *UC-MCM-48–70,* (**d**) *C-MCM-48,* (**e**) *C-MCM-48–50,* (**f**) *C-MCM-48–70,* and **g**) *CC-MCM-48–50*

This was evidence that adding an amine group to the structure caused the d-space, or the distance between the diffraction surfaces, to shrink (Shao et al., 2008). The position of the characteristic Bragg diffraction peaks remained almost constant after the silica-based materials were impregnated with *PEI*, demonstrating that the silica materials' mesoporous structures were retained after the addition of *PEI* (Son et al., 2008).

3.3 Structural Analysis

The structural characteristics of silica-based sorbents were inspected using N_2 adsorption/desorption isotherms at 77 K (Figs. 6 and 7). In addition, isotherm types were investigated to provide a qualitative evaluation of the materials' porous structure. The IUPAC classification's Type IV nitrogen adsorption/

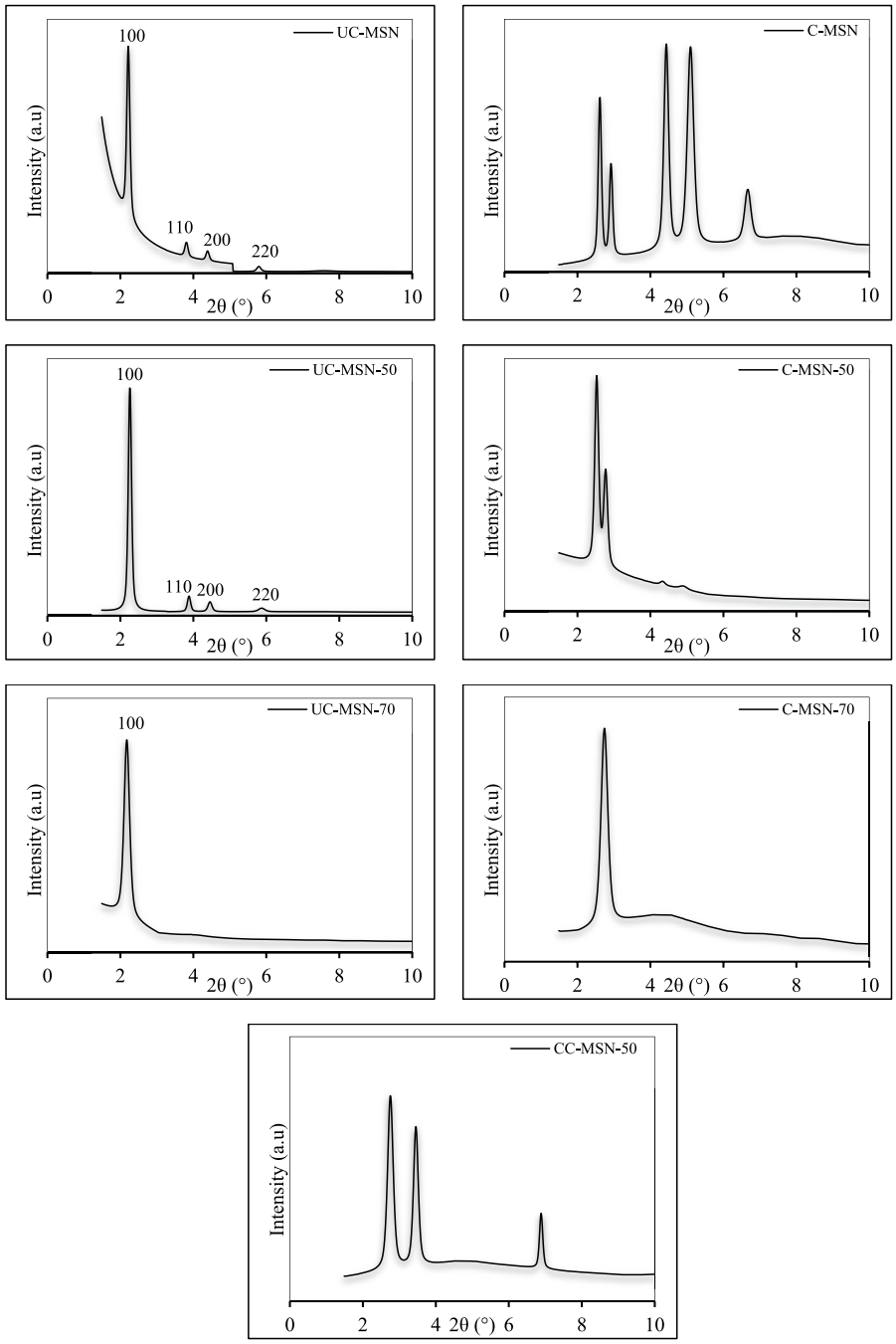

Fig. 4 X-ray diffraction patterns of *MSN*-based adsorbents

desorption isotherm was seen in *MSN* and *MCM-48*-based uncalcined and calcined support materials. It has been noted that the Type H3 hysteresis loops in the *UC-MSN* and *UC-MCM-48* isotherms arise in the presence of plate-like particle clusters that lead to slit-shaped pores and do not display any restrictive adsorption at a high relative pressure (Sing, 1982). *C-MSN* and *C-MCM-48* isotherms exhibited a Type H4 hysteresis loop in the range of approximately $0.40 < P/P_0 < 0.99$, and this hysteresis was characterized by irregular slit-like pores in the structure (Kuila & Prasad, 2013) and secondary (larger) mesopores (Gucbilmez et al., 2012). *C-MCM-48–50* and *UC-MSN–70* were also determined to display

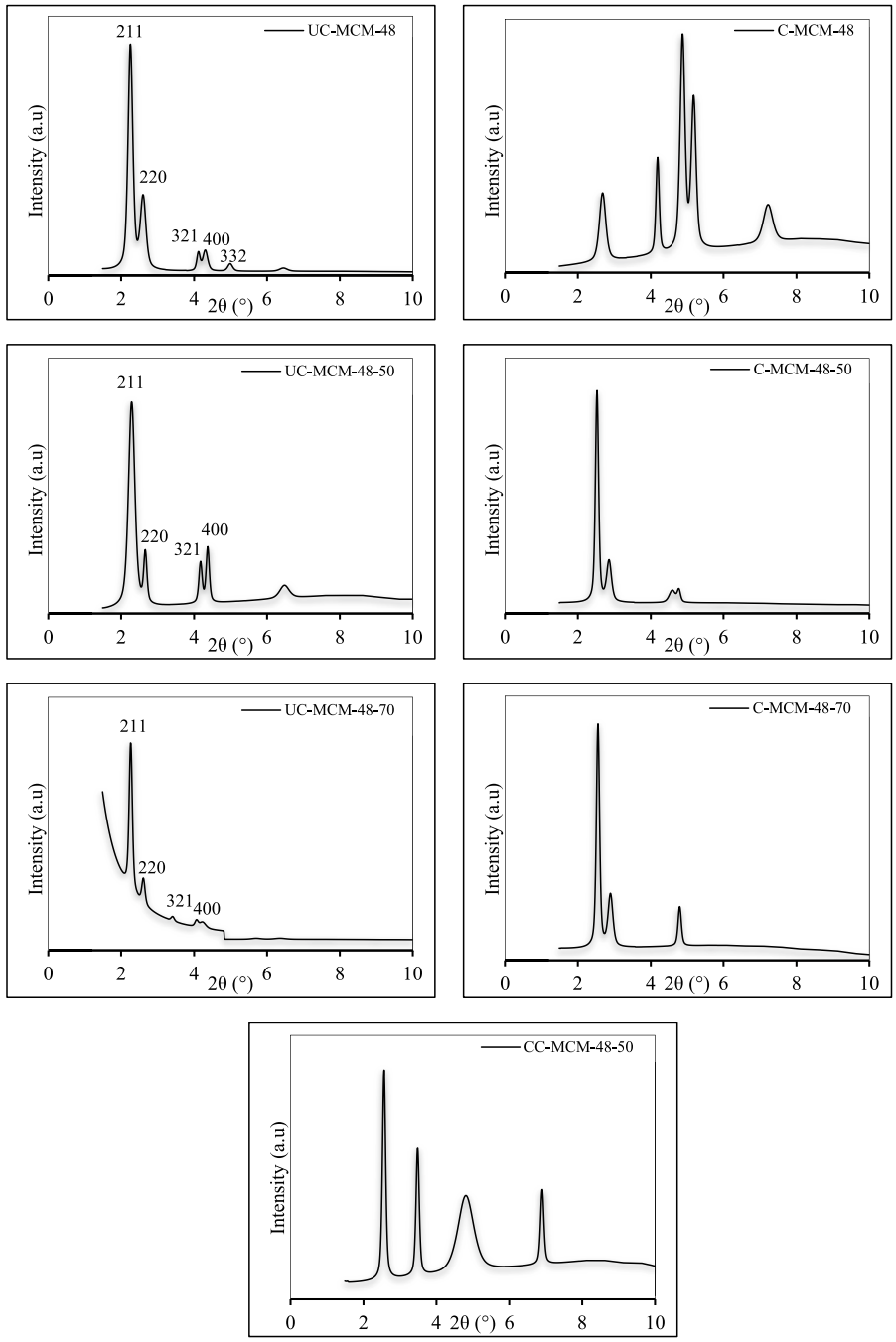

Fig. 5 X-ray diffraction patterns of *MCM-48*-based adsorbents

Type II nitrogen isotherms with H4 hysteresis structure. The *PEI*-loaded adsorbents *UC-MCM-48–50*, *UC-MCM-48–70*, *C-MCM-48–70*, *UC-MSN–50*, *C-MSN–50*, and *C-MSN–70,* on the other hand, showed nearly reversible Type II nitrogen isotherms in contrast to those of silica support materials. The isotherm shape demonstrated that all *PEI*-loaded adsorbents were essentially macroporous and lacked micro/mesopores in the structure. The extremely narrow hysteresis confirmed the presence of small macropores. The *PEI*-loaded materials did not contain micropores, as evidenced by the extremely small amount that was adsorbed at low relative pressure ($P/P_0 < 0.01$) (Kuila & Prasad, 2013). When

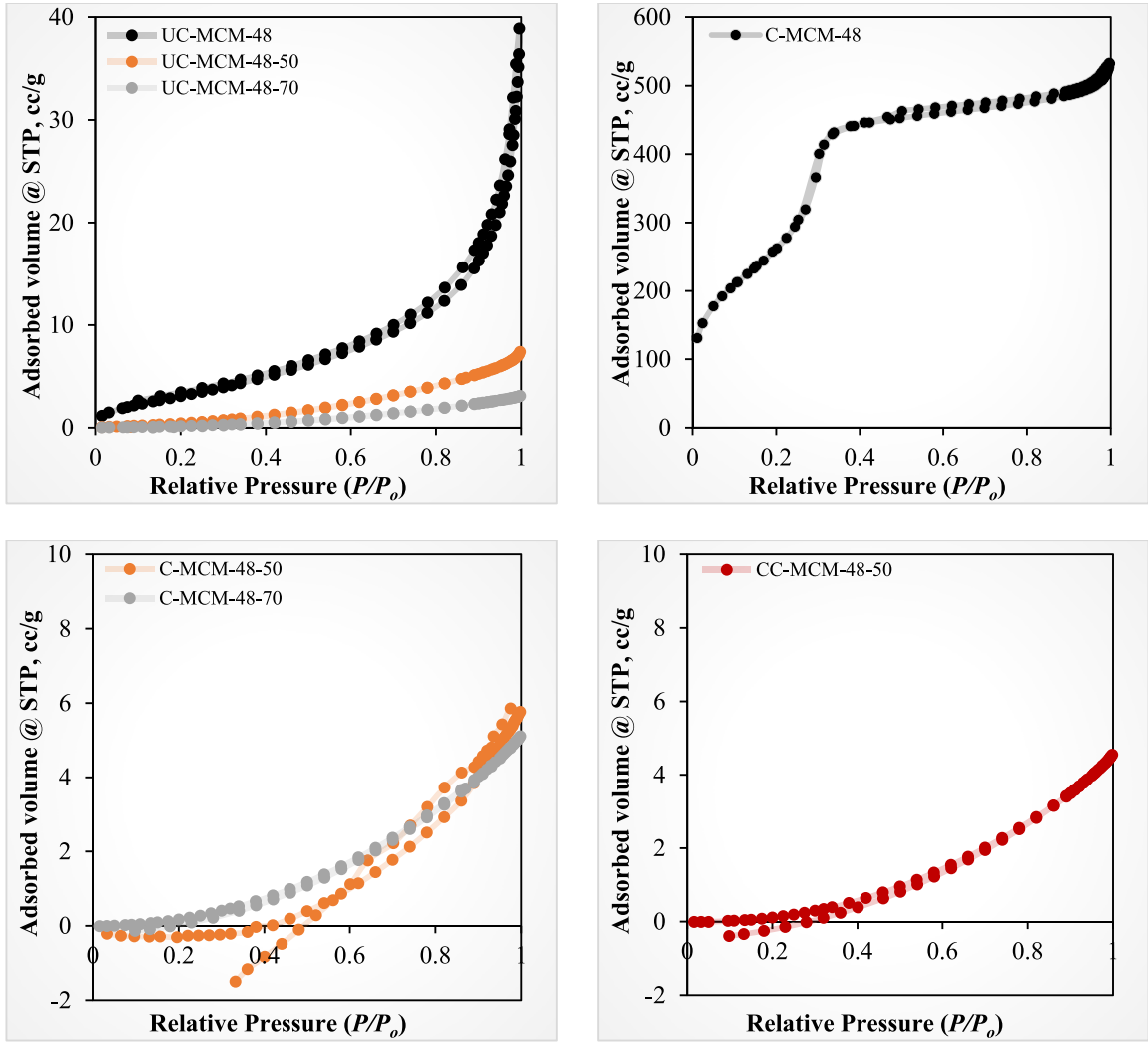

Fig. 6 Nitrogen sorption isotherms of *MCM-48*-based adsorbents

silica support materials were modified with *PEI*, the absence of the hysteresis cycle in the adsorption and desorption branches of adsorbents indicated that the channels in the support material were filled by *PEI* particles (Zhang et al., 2019). It was noted that some adsorbents exhibited open-hysteresis loop isotherms with fractional desorption branches at low relative pressure values. This was because blocked mesopores were prevalent, which discharged at a lower pressure than open pores of similar size (Krzyżak et al., 2020). The irreversibility of the nitrogen adsorption/desorption curves corresponds to open cylindrical pores at both ends and parallel plate-shaped holes in all directions. The fact that the hysteresis loop remained open at low P/P_0 was the most noticeable aspect of this hysteresis. In light of this, it revealed that adsorbents with an open-hysteresis cycle had greater adsorption capacity than adsorbents with closed-loop hysteresis due to their highly developed super micro-pores that were difficult to desorb (Ren et al., 2022).

The pore size distribution curves derived from the BJH method from the desorption branches were also given in Figs. 8 and 9. While most of the *PEI*-loaded sorbents (*UC-MCM-48–50*, *UC-MCM-48–70*, *C-MCM-48–70*, *UC-MSN–70*, *C-MSN–50*, and *C-MSN–70*) showed a wide pore size distribution in the mesopore region with similar properties;

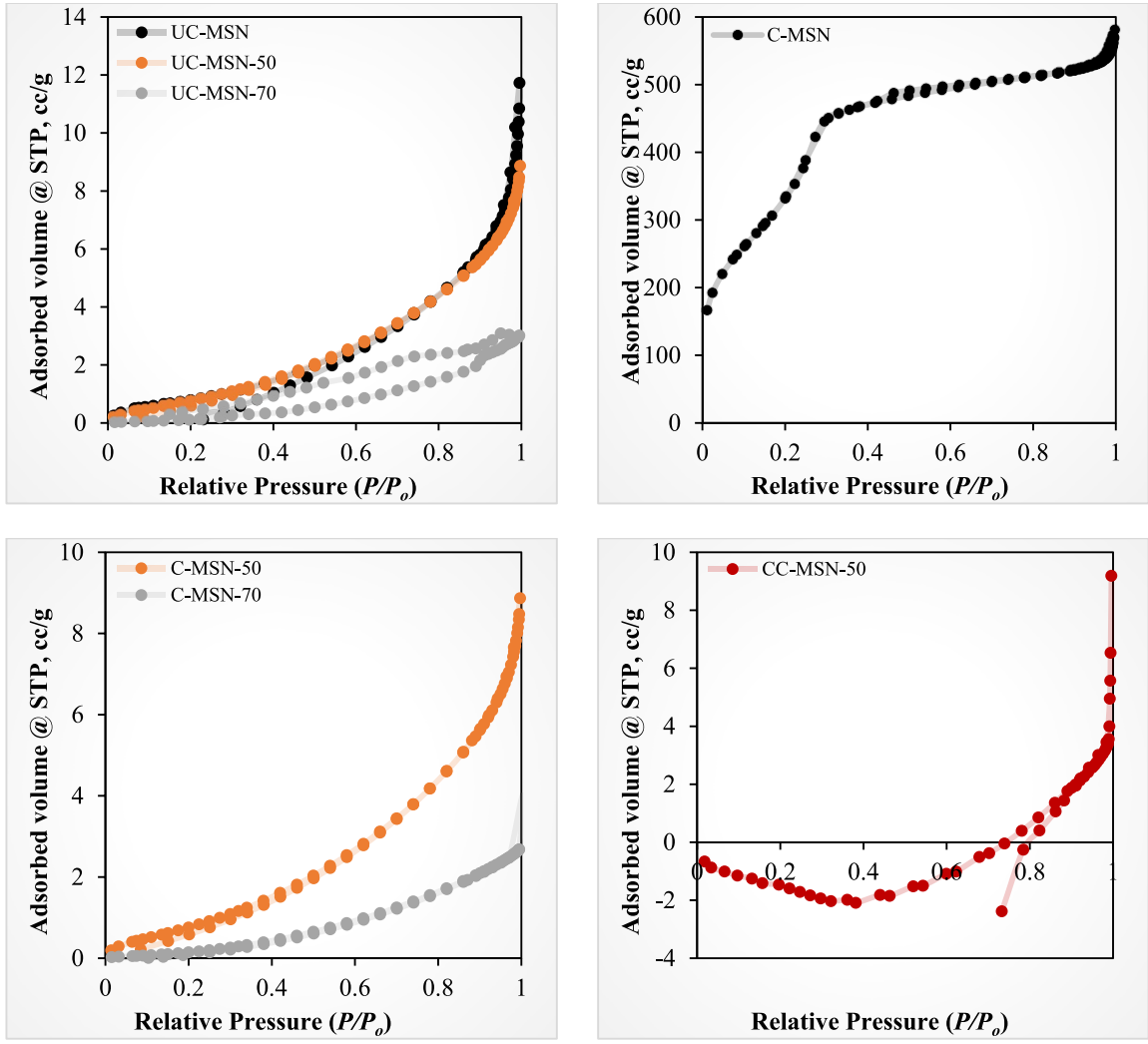

Fig. 7 Nitrogen sorption isotherms of *MSN*-based adsorbents

UC-MCM-48, *C-MCM-48*, *C-MCM-48–50*, *CC-MCM-48–50*, *UC-MSN*, *UC-MSN–50,* and *C-MSN* essentially showed narrow, sharp and homogeneous distribution curve. A bimodal distribution with two distinct peaks at 2.11 and 3.47 nm was observed for *UC-MCM-48*. It was identified that pore sizes were localized around 2.35 and 3.35 nm for *C-MCM-48*, 5.14 nm for *C-MCM-48–50*, 2.10 nm for *CC-MCM-48–50*, 3.36 nm for *UC-MSN*, 3.18 nm for *UC-MSN–50*, 2.50 and 3.86 nm for *C-MSN*. The absence of a noticeable peak in the pore size distribution curves of the sorbents impregnated with *PEI* implied that the amines were virtually filling the channels in the structure (Zhang et al., 2019).

It was specified using the BJH method that the average pore diameters (D_{av}, nm) varied in the mesopore region in the ranges of 2.43–5.12 nm and 2.49–5.62 nm for *MSN*- and *MCM-48*-based sorbents, respectively. The adsorbents' average pore diameters, total pore volumes, and BET surface areas were detailed in Table 2. *UC-MCM-48* and *UC-MSN* had surface areas of around 13.29 m^2/g and 4.07 m^2/g, respectively, while the surface areas of *C-MCM-48* and *C-MSN* were approximately measured as 1153 m^2/g and 1473 m^2/g, respectively. After impregnating *UC-MCM-48* with 50% and 70% by weight amine, it was established that pore blockage caused the surface areas of *UC-MCM-48*-based adsorbents to decrease

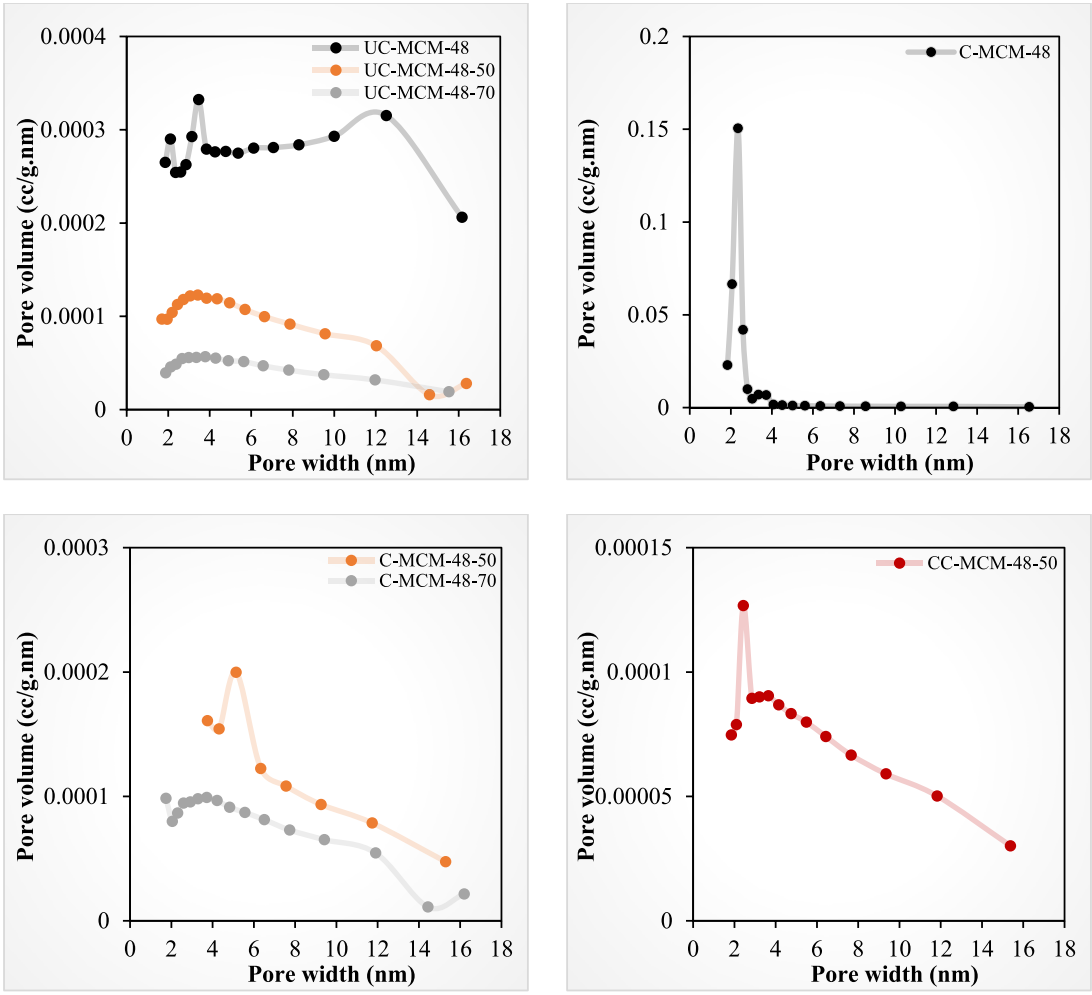

Fig. 8 Pore distribution plots of *MCM-48*-based adsorbents

by 62% and 81%, respectively. Moreover, it was noticed that the total pore volume diminished from 0.0265 cm^3/g to 0.0078 and 0.0035 (Table 2). Similar results were obtained when 50% and 70% by weight of amine were impregnated into *UC-MSN*, which led to reductions in surface area of 11% and 79%, respectively. The calcined materials' surface areas were significantly lowered due to the amine impregnation. For instance, the surface area of *C-MSN* decreased from 1473 m^2/g to 1.76 m^2/g with 70%-*PEI* impregnation. Although the *C-MCM-48* had a surface area of 1153 m^2/g, a BET surface area measurement could not be performed since *PEI* impregnation had blocked the pores. In addition, single-point surface area measurements of *CC-MCM-48–50* and *CC-MSN–50* coded adsorbents produced by *PEI* impregnation after the addition of *CTMABr* surfactant to the calcined *MCM-48* and *MSN* were performed. As a consequence, it was found that the surface area of the adsorbent *CC-MCM-48–50* was 0.75 m^2/g, while *CC-MSN–50*'s surface area could not be established. Since the mesopores of the *PEI*-loaded *C-MCM-48* and *CTMABr*-functionalized *MSN* materials were substantially covered with *PEI*, nitrogen had limited access to the pores at liquid nitrogen temperature hence details on the fundamental textural properties of these materials could not be inferred from N_2 sorption isotherms. However, it was determined that *CC-MSN–50* and *CC-MCM-48–50* had mean pore diameter values of 14.64 nm and 4.89 nm, respectively.

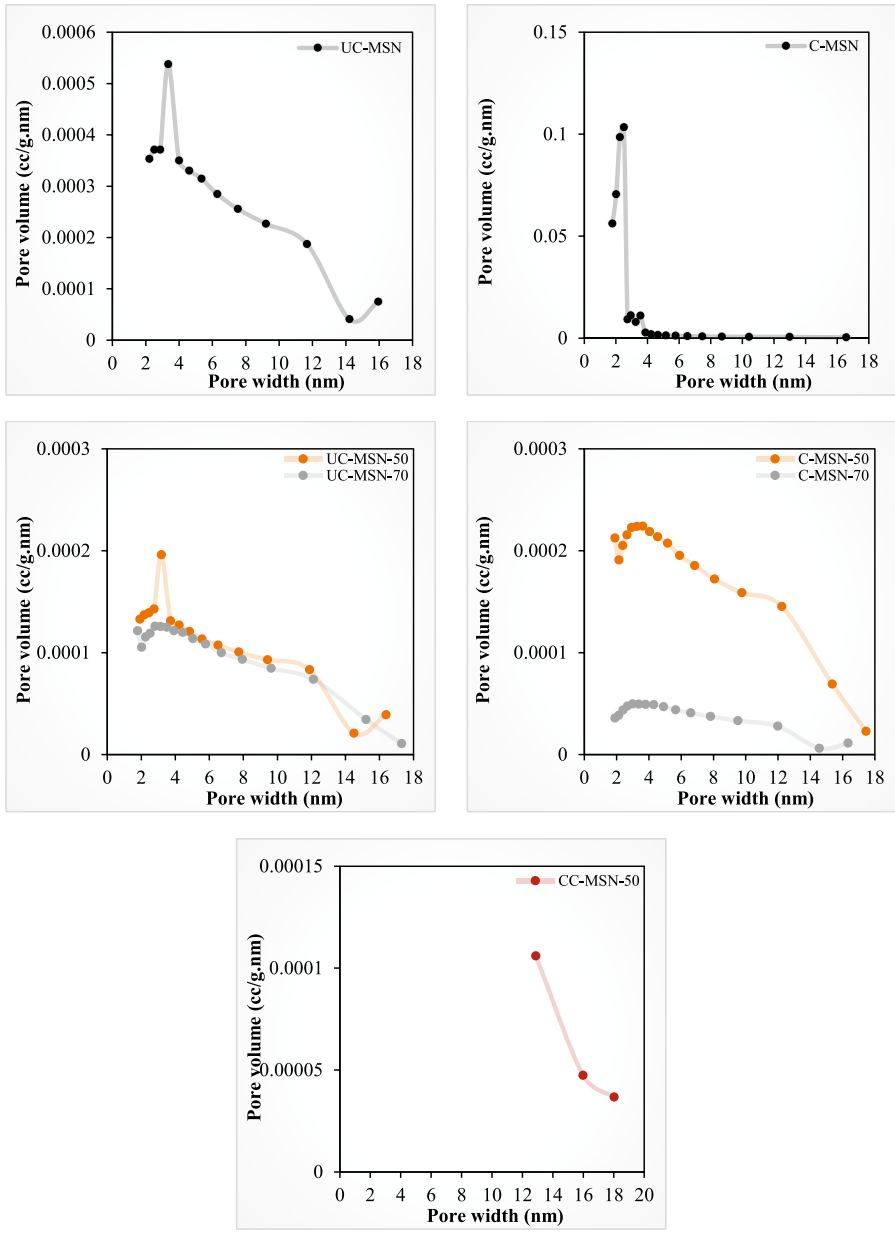

Fig. 9 Pore distribution plots of *MSN*-based adsorbents

3.4 FT-IR Spectrum

When the spectrum of pure polyethyleneimine in Fig. 10 was analyzed, peaks were seen at wavenumbers of 3420, 2925, and 2852 cm^{-1}, confirming the presence of -NH or -CH_2 radicals in the chemical structure of *PEI* (Xing et al., 2014). The two bands at 2851 and 2921 cm^{-1} in the FT-IR spectrum of *UC-MCM-48* and *UC-MSN* (Fig. 10) corresponded to the symmetric and asymmetric stretching vibrations of the CH_2 groups, respectively (Taba et al., 2017). For the bending vibrations of –O–H and C-H, two additional peaks were identified at 1650 and 1460 cm^{-1}. The presence of surfactants utilized as structure-directing agents was revealed by the peaks in the spectrum linked to C-H stretching and bending vibrations. Sharp peaks at 1212 and 1024 cm^{-1} were associated with Si–O–Si groups'

Table 2 Structural properties of support materials and *PEI*-loaded adsorbents

Adsorbent codes	S_{BET} (m^2/g)	V_{total} (cm^3/g)	D_{av} (nm)
MSN-based materials			
UC-MSN	4.07	0.0083	4.83
UC-MSN–50	3.64	0.0084	5.01
UC-MSN–70	0.86	0.0190	5.12
C-MSN	1472.84	0.9269	2.43
C-MSN–50	8.28	0.0156	5.05
C-MSN–70	1.76	0.0031	5.01
MCM-48-based materials			
UC-MCM-48	13.29	0.0265	5.62
UC-MCM-48–50	5.05	0.0078	4.82
UC-MCM-48–70	2.57	0.0035	4.98
C-MCM-48	1153.25	0.7969	2.49
C-MCM-48–50	–	0.0065	6.64
C-MCM-48–70	–	0.0060	4.82
CTMABr-functionalized materials	$S_{single\ point}$ (m^2/g)	V_{total} (cm^3/g)	D_{av} (nm)
CC-MSN–50	-	0.0028	14.64
CC-MCM-48–50	0.75	0.0053	4.89

asymmetric stretching vibrations (Taba et al., 2018). The defective Si–OH vibration in silicate lattice appeared at 956 cm^{-1}. The weak bands at 778 and 430 cm^{-1} corresponded to the symmetrical stretching vibration of Si–O–Si bonds and their bending mode, respectively (Venkatachalam et al., 2012). Free silica may also be present in the band about 795 cm^{-1}. Similar bands and bond stretching characteristics were also visible in the spectra of the calcined adsorbents. All organic group bands in the calcined pure support materials (*C-MCM-48* and *C-MSN* not impregnated with *PEI*) had disappeared, proving that the surfactant was eliminated completely from the samples during the calcination process (Loganathan et al., 2013).

All *PEI*-impregnated materials (Fig. 10) were identified to exhibit a broad envelope between 3600 and 3000 cm^{-1}, indicating the –OH stretching vibration of water (Aghaei et al., 2014). The wide band of the water's –OH stretching vibration masked the stretching vibration peak of defective Si–O–H groups (Malhis et al., 2018). Moreover, the peaks at 1560 cm^{-1} in the FT-IR spectra of the *PEI*-loaded sorbents indicated the amino bending vibration and confirmed the successful doping of the amine groups. Finally, the peak arising at 1665 cm^{-1} verified the existence of the amino group (Du et al., 2013). The formation of additional peaks in the 1650–1300 cm^{-1} range upon impregnation provided evidence for *PEI*'s existence in the adsorbent. The specific peaks at 1315 and 1400 cm^{-1} corresponded to the skeletal vibration of the carbamate ($NCOO^-$) and the stretching vibration of the –NC group of carbamates. The stretching vibration of C–H and the bending vibration of CH_2 in the *PEI* chain were defined by 2950–2860 cm^{-1} and 1460 cm^{-1} peaks, respectively (Kishor & Ghoshal, 2016). Further evidence that polyethyleneimine adhered on silica support materials were the peaks of 3200 cm^{-1}, 1030 cm^{-1} (C-N stretching vibration), 1606 cm^{-1} (N–H bending), and 550 cm^{-1} (N–H wagging) (Ahmad et al., 2018).

3.5 CO_2 Adsorption Performances

Figure 11a-d illustrated the isotherms of the analyses carried out at 75 °C to investigate the CO_2 adsorption capacity of *MCM-48*- and *MSN*-based mesoporous adsorbents. The test results revealed that, while *UC-MCM-48* had an adsorption capacity of 0.48 mmol/g, *UC-MCM-48–50* adsorbent with 50% polyethyleneimine had the highest capacity for CO_2 holding at 2.26 mmol/g. The CO_2 sorption capacities of 50% and 70% *PEI* functionalized materials were measured to be 4.71 and 3.35 times that of the synthesized *UC-MCM-48*, respectively. These values were found to be inversely related to the adsorbents' surface area. Similarly, the CO_2 sorption capacity of *C-MCM-48* was also measured to be 0.36 mmol/g, while *C-MCM-48–50* and *C-MCM-48–70* adsorbed CO_2 at 2.03 mmol/g and 1.16 mmol/g, respectively.

The adsorption capacities of *UC-MSN* and *C-MSN* were 0.26 mmol/g and 0.50 mmol/g, respectively (Fig. 11c and d). *UC-MSN–50* had a CO_2 sorption capacity of 3.31 mmol/g, which was 12.73 times that of *UC-MSN* and 1.44 times that of *UC-MSN–70*. Finally, it was reported that doping polyethyleneimine at 50 and 70% proportions to the *C-MSN* formed adsorbents with remarkably similar adsorption capabilities (1.85 mmol/g and 1.89 mmol/g). The CO_2 adsorption capabilities of the *CC-MSN–50* and *CC-MCM-48–50* adsorbents were measured at 75 °C as 1.83 mmol/g and 1.95 mmol/g, respectively, following the CO_2 adsorption curves shown in Fig. 11e. These adsorbents were produced by

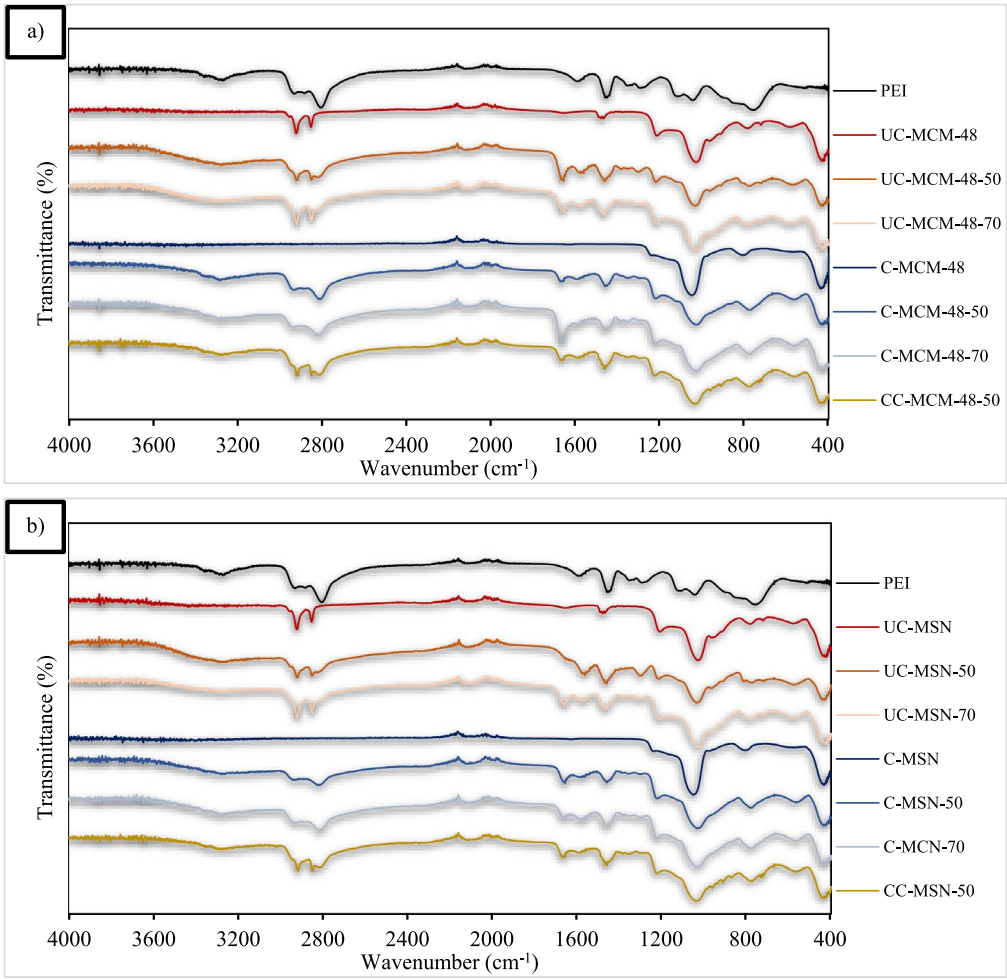

Fig. 10 FT-IR spectrum of **a**) *MCM-48*- and **b**) *MSN*-based adsorbents compared to *PEI*

adding the *CTMABr* surfactant before the impregnation of the amine group to the calcined support materials. The CO_2 sorption capabilities of the two optimally selected adsorbents at 100 °C were measured to evaluate the temperature effect (Fig. 11f). Consequently, *UC-MSN–50* adsorbed CO_2 at remarkably similar levels, namely 3.31 mmol/g and 3.43 mmol/g at 75 °C and 100 °C, respectively. It was established that the sorption capability of *UC-MCM-48–50* (2.26 mmol/g at 75 °C) lowered to 1.72 mmol/g at 100 °C with the rising temperature. When the CO_2 adsorption capacities of *PEI*-modified *MCM-48* and *MSN* amin-silica composites developed in this study were compared with the values of various *PEI*-functionalized silica-based materials presented in Table 3. The results revealed that the *PEI*-modified *MCM-48* and *MSN* composites were effective CO_2 adsorbents due to their enhanced CO_2 capture capability. It was also conspicuous that *PEI*-functionalized silica materials (especially *UC-MSN–50*: 3.31 mmol/g @ 75 °C and *UC-MCM-48–50*: 2.26 mmol/g @ 75 °C) were suitable for use as a prospective CO_2 adsorbent concerning their competitively high CO_2 adsorption capacity (3.31 mmol/g).

In summary, support materials with mesoporous and targeted crystalline structures were prepared as proven by nitrogen physisorption and x-ray diffraction analyses; the presence of surface functional groups formed by *PEI* modification was determined by FTIR analysis; SEM analysis concluded that the silica support surface was coated with *PEI*; and finally, amine-silica composite adsorbents exhibited

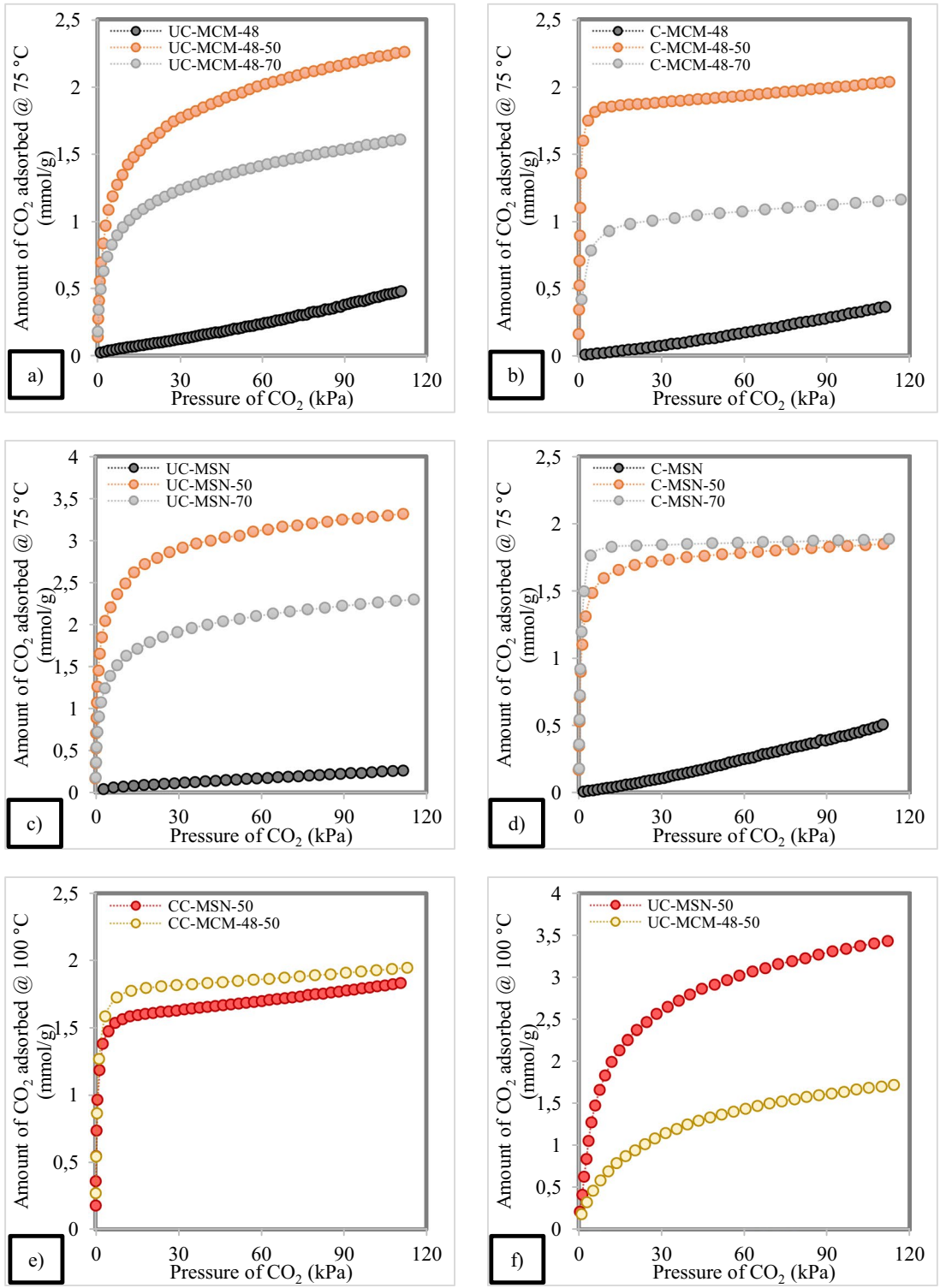

Fig. 11 CO_2 adsorption isotherms of *MCM-48*- and *MSN*-based materials

Table 3 Comparing the ability of *PEI*-functionalized silica-based materials to adsorb CO_2

Support Type	*PEI*-loading (wt.%)	Adsorption capacity (mmol CO_2/g-adsorbent)	References
FS	40	2.16	(Zhao et al., 2019)
HMS-C	20–70	0.59–2.61	(Chen et al., 2010)
KIT-6	10–50	0.34–3.07	(Son et al., 2008)
KIT-6	40	0.55	(Zhao et al., 2019)
MCM-41	50	2.52	(Son et al., 2008)
MCM-41	40	0.71	(Zhao et al., 2019)
MCM-41	10–50	0.56–2.20	(Sanz-Pérez et al., 2017)
MCM-48	50	2.70	(Son et al., 2008)
MCM-48-C	10–50	1.06–2.16	(Qian et al., 2019)
MCM-48-W	10–50	1.46–2.59	(Qian et al., 2019)
SBA-15	50	2.89	(Son et al., 2008)
SBA-15	50	1.72	(Sanz-Pérez et al., 2017)
SBA-15	20–60	0.90–1.40	(Henao et al., 2020)
SBA-15	30	1.49	(Sanz-Pérez et al., 2016)
SBA-15	40	1.37	(Zhao et al., 2019)
SBA-16	50	2.93	(Son et al., 2008)

successful performance in the CO_2 adsorption process. Thus, *i)* type of silica support material, *ii)* calcination status of support material, *iii) PEI* loading ratio, *iv)* surfactant additive, and *v)* adsorption temperature parameters were comparatively examined, and the adsorption mechanism was explained through adsorption isotherms and thermodynamics in Section 3.6.

3.6 Adsorption Isotherms and Thermodynamics

The results of a study on four pure gas isotherm models for CO_2 adsorption equilibrium were summarized in Table 4. Comparisons between CO_2 adsorption isotherms predicted through various isotherm models and experimental data for *MCM-48*- and *MSN*-based adsorbents were given in Figs. 12 and 13. The affinity between adsorbent and adsorbate molecules was represented by the Langmuir and Freundlich isotherm constants, k_L and k_F, which increased with the rise in CO_2 adsorption capacity (Fatima et al., 2023). For *UC-MCM-48–50* and *UC-MSN–50*, both constant values decreased at higher temperatures (100 °C), suggesting physisorption behavior. In contrast, calcined and *PEI*-modified sorbents had greater k_L and k_F values. A rise in the isotherm constant values suggested that *PEI* functionalities of calcined supports caused significant chemical interactions in addition to the physisorption of CO_2. For pressures up to 60 kPa, there was an excellent correlation between experimental isotherms and predicted curves (mostly Langmuir and Temkin, possibly Freundlich); however, the Langmuir model fitted the data better across a wider pressure range. The deviation from the model hypothesis at elevated pressures appeared to make it more difficult to predict the adsorption capacity using the Freundlich and Temkin equations. The coordinated fit order of the isotherm models to the experimental data was Langmuir > Temkin > Freundlich > Dubinin-Radushkevich, as specified by the R^2 values in Table 4. Overall, the significant fit between experimental data and theoretical predictions for Langmuir isotherms was demonstrated by the high correlation coefficients (R^2 > 0.993). For *UC-MCM-48–50*, the Langmuir isotherm's value of q_m indicated the greatest monolayer coverage, which reduced as the temperature rose, indicating that the adsorption process was exothermic. The Freundlich model's heterogeneity factor (n) values were higher than 1 in all amine-silica composite adsorbents, indicating that physisorption was the primary adsorption mechanism. The spontaneous character of the adsorption process was confirmed by the Freundlich heterogeneity parameter ($1/n$) values being smaller than 1. Furthermore, these values change significantly following calcination before

Table 4 Isotherm model parameters for CO_2 adsorption of amin-modified silica sorbents (q_m: mmol/g; k_L: 1/kPa; k_F: mmol/(g.(kPa)$^{1/n}$); k_{DR}: mmol^2/kJ^2; E: kJ/mol; k_T: mmol/g.kPa; b_t: kJ/mol)

T (°C)	Adsorbent codes	Langmuir Isotherm			Freundlich Isotherm			Dubinin-Radushkevich Isotherm				Temkin Isotherm		
		q_m	k_L	R^2	n	k_F	R^2	q_m	k_{DR}	E	R^2	k_T	b_t	R^2
	MSN-based materials													
75	*UC-MSN–50*	3.3168	0.3839	0.9987	3.3750	1.0055	0.8654	2.5800	4.7E+04	3.2594	0.8489	22.737	6.66	0.9926
	UC-MSN–70	2.3089	0.2547	0.9975	3.4305	0.6716	0.9106	1.7595	5.3E+04	3.0777	0.7798	15.266	9.35	0.9979
	C-MSN–50	1.8467	0.7422	0.9997	4.1876	0.7201	0.8298	1.5995	3.7E+04	3.6904	0.8799	68.567	13.24	0.9532
	C-MSN–70	1.8897	1.4048	1.0000	4.2105	0.7624	0.7461	1.7731	5.8E+04	2.9357	0.9777	74.664	12.70	0.8790
100	*UC-MSN–50*	3.6590	0.0949	0.9980	2.2857	0.5265	0.9170	2.3836	2.4E+05	1.4563	0.6196	1.6689	4.72	0.9922
	MCM-48-based materials													
75	*UC-MCM-48–50*	2.3079	0.1486	0.9951	3.0497	0.5425	0.9384	1.6873	5.9E+04	2.9142	0.6650	7.1927	8.76	0.9916
	UC-MCM-48–70	1.6461	0.1323	0.9937	3.5511	0.4544	0.9641	1.2428	5.5E+04	3.0231	0.6258	8.4368	12.75	0.9882
	C-MCM-48–50	2.0178	0.7005	0.9993	4.6948	0.8570	0.7496	1.8615	3.8E+04	3.6416	0.9377	177.10	13.53	0.8898
	C-MCM-48–70	1.1712	0.2540	0.9986	5.6402	0.5242	0.8740	1.0525	2.3E+05	1.4765	0.8912	45.413	21.15	0.9499
100	*UC-MCM-48–50*	1.9673	0.0495	0.9934	2.1925	0.2187	0.9807	1.2136	4.9E+05	1.0023	0.5496	0.7602	8.31	0.9747
	CTMABr-functionalized materials													
75	*CC-MSN–50*	1.8149	0.4202	0.9983	4.6555	0.7415	0.7774	1.6469	5.1E+04	3.1446	0.9449	102.83	14.50	0.9215
	CC-MCM-48–50	1.9402	0.6474	0.9995	4.6729	0.8104	0.7742	1.8053	6.3E+04	2.8098	0.9586	91.083	13.10	0.8937

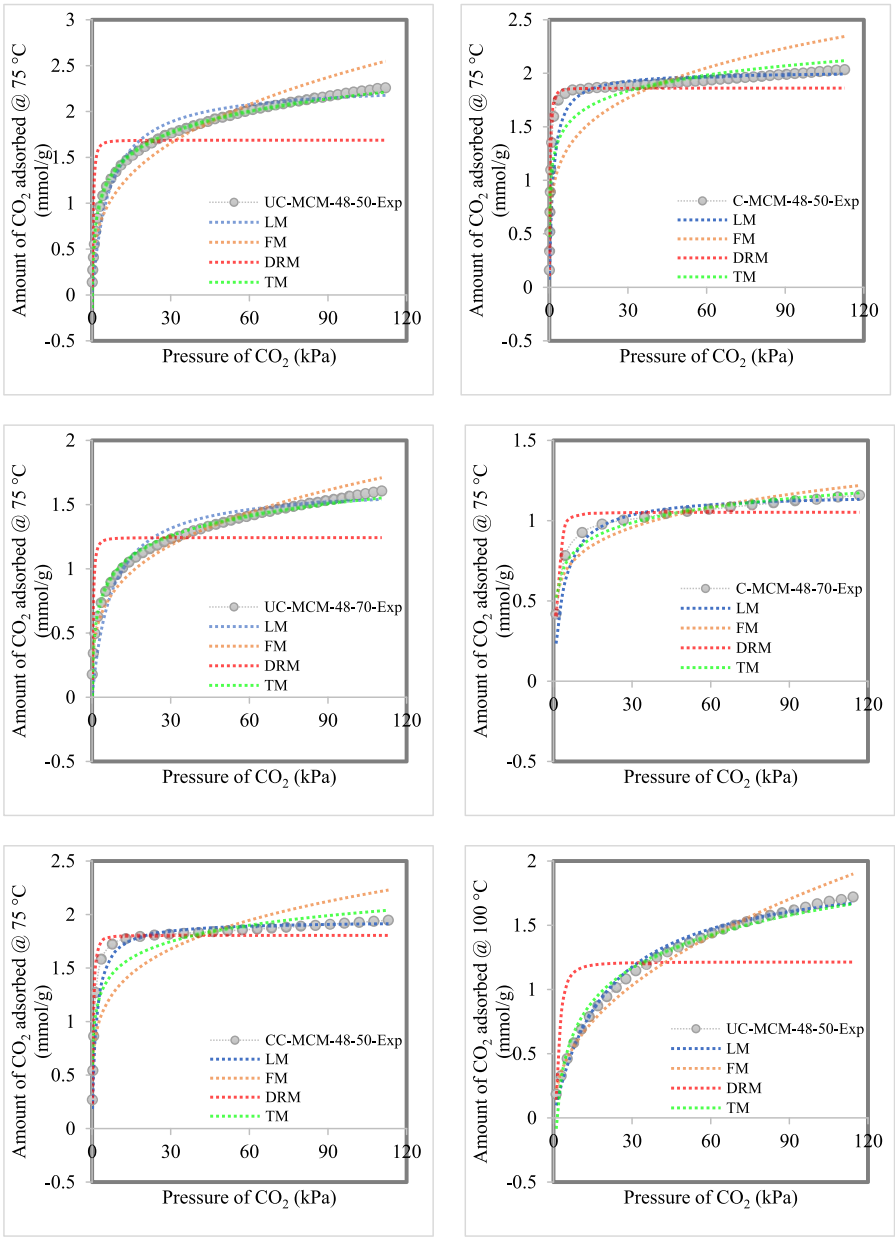

Fig. 12 Isotherm modeling of CO_2 adsorption: a comparison between CO_2 adsorption isotherms predicted through various isotherm models and experimental data for *MCM-48*-based adsorbents (*S-x-Exp*: Experimental data, *LM*: Langmuir, *FM*: Freundlich, *DRM*: Dubinin-Radushkevich, and *TM*: Temkin isotherm models fitting)

functionalization, suggesting that the adsorbent's surfaces were energetically heterogeneous when applying *PEI* impregnation after calcination. For the *PEI*-silica composite adsorbents, the mean free energy of adsorption (E) determined by the D-R model was less than 8 kJ/mol, confirming that physical forces controlled the adsorption process and that it did not generate a significant amount of heat. *PEI*-modified *UC-MCM-48* and *UC-MSN* sorbents' Temkin model correlation coefficients (R^2 ~ 99) revealed that the Temkin isotherm fitted the experimental data quite well, confirming the adsorbents' energetically heterogeneous surfaces. The nature of adsorbate-adsorbent interaction was also indicated by the Temkin model parameter b, which expressed bonding energy. The physical adsorption was confirmed by bonding energies up to 20 kJ/mol (Tiwari et al., 2018). For *UC-MCM-48–50* and *UC-MSN–50*, the Temkin constant (k_T) values declined with temperature, suggesting that the CO_2 molecules had a physical interaction

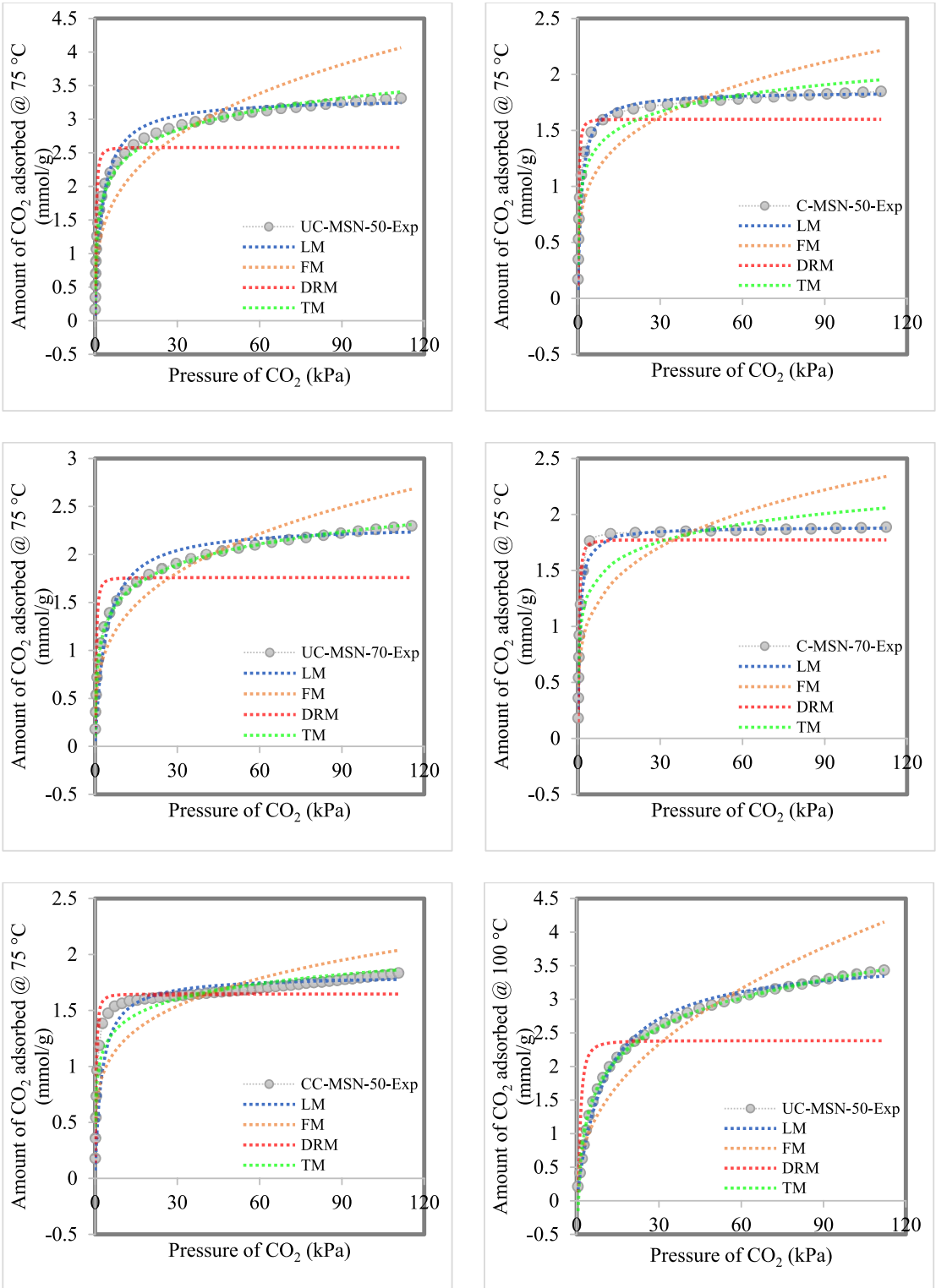

Fig. 13 Isotherm modeling of CO_2 adsorption: a comparison between CO_2 adsorption isotherms predicted through various isotherm models and experimental data for *MSN*-based adsorbents (*S-x-Exp*: Experimental data, *LM*: Langmuir, *FM*: Freundlich, *DRM*: Dubinin-Radushkevich, and *TM*: Temkin isotherm models fitting)

(potentially a weak van der Waals interaction) with the uncalcined silica-amine composites. Furthermore, k_T values for calcined silica-amine composites revealed an enhanced interaction between *PEI* functionalities loaded after calcination and CO_2.

The thermodynamic constant values at different temperatures for *UC-MSN–50* and *UC-MCM-48–50* were given in Table 5. Table 4 displayed that the k_L values of *UC-MSN–50* and *UC-MCM-48–50* diminished with increasing temperature, implying an exothermic adsorption mechanism. The thermodynamic study's positive ΔG° values at 75 and 100 °C implied a thermodynamically non-spontaneous adsorption reaction. The exothermic characteristics of the CO_2 adsorption processes for both amine-silica composites were corroborated by the negative ΔH° values (−60.312 and −47.447 kJ/mol). The ΔH° value of less than 20 kJ/mol signifies a physisorption process, while the value falls between 80 and 200 kJ/mol for chemical adsorption (Rashidi et al., 2016; Singh et al., 2018). The adsorption process is typically considered to be dominated by chemical adsorption if the enthalpy change is more than 40 kJ/mol. ΔS° values were found to be −0.181 and −0.152 kJ/mol.K, in this instance, the relatively low ΔS° number denoted an insignificant entropy change. The negative value of ΔS° meant that the irregularity of the adsorption process was reduced. It also signified that the adsorbate molecules were situated and controlled at particular adsorbent sites.

4 Conclusions

Within the scope of the study, the amine-impregnated silica materials, known to have high CO_2 adsorbing capacities in gas phase systems, were synthesized then their characteristic properties were clarified using analyses such as x-ray diffraction, FT-IR spectroscopy, nitrogen sorption, and scanning electron microscopy. Uncalcined and calcined (*UC-MCM-48*, *UC-MSN*, *C-MCM-48*, and *C-MSN*) silica support materials were impregnated with polyethyleneimine at different proportions (50% and 70% by weight). When the impact of the impregnation procedure on the adsorbent characteristics was investigated, it was revealed that the surface area decreased significantly as the *PEI* loading ratio increased. The characteristic diffraction peaks in the (1 0 0) plane of *MSN* and the (2 1 1) plane of *MCM-48* associated with the crystal structures were also preserved even after the amine group was incorporated into the silica-based materials. When the gaseous pollutant CO_2 adsorption capabilities of adsorbents were examined, it was noted that the support materials without *PEI* had low capacities (*UC-MCM-48*: 0.48 mmol/g, *MCM-48*: 0.36 mmol/g, *UC-MSN*: 0.26 mmol/g, *C-MSN*: 0.50 mmol/g), and the capacity values had improved after the addition of the amine group to the structure as 2.26 mmol/g and 3.31 mmol/g for *UC-MCM-48–50* and *UC-MSN–50*, respectively. Based on the CO_2 adsorption plots at 75 °C, the capacities of *CC-MSN–50* and *CC-MCM-48–50* produced by mixing *CTMABr* surfactant to the calcined material, and then adding *PEI* were 1.83 mmol/g and 1.95, respectively. When the temperature effect on the CO_2 adsorption ability was analyzed, it was specified that *UC-MSN–50* and *UC-MCM-48–50* with optimum holding values exhibited capacities as 3.43 mmol/g and 1.72 mmol/g as a result of increasing temperature. Within the scope of this study, it was concluded that adsorbents generated by impregnating *PEI* on different mesoporous silica-based supports could be utilized for CO_2 capture in gas phase adsorption systems, and the adsorption performance could be improved by changing the support material type, calcination state, amine impregnation ratio and applying surfactant doping.

Table 5 Thermodynamics parameters of CO_2 adsorption on *UC-MSN–50* and *UC-MCM-48–50*

Adsorbent code	Temperature (K)	ΔG° (kJ/mol)	ΔH° (kJ/mol)	ΔS° (kJ/mol.K)
UC-MSN–50	348	2.770	−60.312	−0.181
	373	7.302		
UC-MCM-48–50	348	5.517	−47.447	−0.152
	373	9.322		

Acknowledgements The authors would like to thank the Bilecik Seyh Edebali University Scientific Research Projects Coordination Unit under Grant Number 2021-01.BŞEÜ.01-06 for financial support.

Authors Contribution Adife Seyda Yargic: Conceptualization, Investigation, Methodology, Project Administration, Visualization, Writing-Review&Editing. Mustafa Sener: Formal Analysis, Writing-Original Draft.

Funding Open access funding provided by the Scientific and Technological Research Council of Türkiye (TÜBİTAK). This research was financially supported by the Bilecik Seyh Edebali University Scientific Research Projects Coordination Unit under Grant Number 2021–01.BŞEÜ.01–06.

Data Availability The authors declare that the data supporting the findings of this study are available within the paper. Should any raw data files be needed in another format they are available from the corresponding author upon reasonable request. Source data are provided in this paper.

Declarations

Competing Interest The authors report no declarations of interest.

References

Aghaei, H., Nourbakhsh, A. A., Karbasi, S., JavadKalbasi, R., Rafienia, M., Nourbakhsh, N., Bonakdar, S., & Mackenzie, K. J. (2014). Investigation on bioactivity and cytotoxicity of mesoporous nano-composite MCM-48/hydroxyapatite for ibuprofen drug delivery. *Ceramics International, 40*(5), 7355–7362.

Ahmad, H., Umar, K., Ali, S. G., Singh, P., Islam, S. S., & Khan, H. M. (2018). Preconcentration and speciation of arsenic by using a graphene oxide nanoconstruct functionalized with a hyperbranched polyethyleneimine. *Microchimica Acta, 185*, 1–7.

Al-Ghussain, L. (2019). Global warming: Review on driving forces and mitigation. *Environmental Progress & Sustainable Energy, 38*(1), 13–21.

Alsyouri, H. M., Abu-Daabes, M. A., Alassali, A., & Lin, J. Y. (2013). Ordered mesoporous silica prepared by quiescent interfacial growth method-effects of reaction chemistry. *Nanoscale Research Letters, 8*, 1–15.

Chai, S. H., Liu, Z. M., Huang, K., Tan, S., & Dai, S. (2016). Amine functionalization of microsized and nanosized mesoporous carbons for carbon dioxide capture. *Industrial and Engineering Chemistry Research, 55*(27), 7355–7361.

Chang, F. Y., Chao, K. J., Cheng, H. H., & Tan, C. S. (2009). Adsorption of CO_2 onto amine-grafted mesoporous silicas. *Separation and Purification Technology, 70*(1), 87–95.

Chegeni, A., Babaeipour, V., Fathollahi, M., & Hosseini, S. G. (2022). Modeling of CO_2 Adsorption Isotherms, Kinetics and Thermodynamics Equilibrium, and the Brunauer-Emmett-Teller Analysis onto KO_2 Pellets. *Journal of Cluster Science, 33*(5), 2167–2178.

Chen, C., Son, W. J., You, K. S., Ahn, J. W., & Ahn, W. S. (2010). Carbon dioxide capture using amine-impregnated HMS having textural mesoporosity. *Chemical Engineering Journal, 161*(1–2), 46–52.

Das, D., Lee, J. F., & Cheng, S. (2004). Selective synthesis of Bisphenol-A over mesoporous MCM silica catalysts functionalized with sulfonic acid groups. *Journal of Catalysis, 223*(1), 152–160.

Das, S., Manam, J., & Sharma, S. K. (2016). Role of rhodamine-B dye encapsulated mesoporous SiO_2 in color tuning of $SrAl_2O_4$: Eu^{2+}, Dy^{3+} composite long lasting phosphor. *Journal of Materials Science: Materials in Electronics, 27*, 13217–13228.

do Nascimento, A. R., Medeiros, R. D. A., Melo, M. D. F., Melo, D. D. A., & de Souza, M. J. B. (2016). Optimization of MCM-48 synthesis using factorial design. *Cerâmica., 62*, 413–417.

Du, Y., Du, Z., Zou, W., Li, H., Mi, J., & Zhang, C. (2013). Carbon dioxide adsorbent based on rich amines loaded nano-silica. *Journal of Colloid and Interface Science, 409*, 123–128.

El-Desouky, M. G., Shahat, A., El-Bindary, A. A., & El-Bindary, M. A. (2021). Description, kinetic and equilibrium studies of the adsorption of carbon dioxide in mesoporous iron oxide nanospheres. *Biointerface Research in Applied Chemistry, 12*, 3034–3054.

Fatima, S. S., Borhan, A., Ayoub, M., & Ghani, N. A. (2023). Modeling of CO_2 Adsorption on Surface-Functionalized Rubber-Seed Shell Activated Carbon: Isotherm and Kinetic Analysis. *Processes, 11*(10), 2833.

Fernandez, D. C., Morales, D. S., Jiménez, J. R., & Fernández-Rodriguez, J. M. (2022). CO_2 adsorption by organohydrotalcites at low temperatures and high pressure. *Chemical Engineering Journal, 431*, 134324.

Fernández-Miranda, N., Garcia, S., Lopez-Anton, M. A., Martínez-Tarazona, M. R., Sanz-Pérez, E. S., & Maroto-Valer, M. M. (2017). Effect of Hg on CO_2 capture by solid sorbents in the presence of acid gases. *Chemical Engineering Journal, 312*, 367–374.

Friedlingstein, P., Houghton, R. A., Marland, G., Hackler, J., Boden, T. A., Conway, T. J., Canadell, J. G., Raupach, M.

R., Ciais, P., & Le Quéré, C. (2010). Update on CO_2 emissions. *Nature Geoscience, 3*(12), 811–812.

Garnier, C., Finqueneisel, G., Zimny, T., Pokryszka, Z., Lafortune, S., Défossez, P. D. C., & Gaucher, E. C. (2011). Selection of coals of different maturities for CO_2 Storage by modelling of CH_4 and CO_2 adsorption isotherms. *International Journal of Coal Geology, 87*(2), 80–86.

Gholidoust, A., Atkinson, J. D., & Hashisho, Z. (2017). Enhancing CO_2 adsorption via amine-impregnated activated carbon from oil sands coke. *Energy & Fuels, 31*(2), 1756–1763.

Gucbilmez, Y., Yargic, A. S., & Calis, I. (2012). A comparative characterization of the HPA-MCM-48 type catalysts produced by the direct hydrothermal and room temperature synthesis methods. *Journal of Nanomaterials, 2012*, 28–28.

Guo, X., Ding, L., Kanamori, K., Nakanishi, K., & Yang, H. (2017). Functionalization of hierarchically porous silica monoliths with polyethyleneimine (PEI) for CO_2 adsorption. *Microporous and Mesoporous Materials, 245*, 51–57.

Han, L., Zhou, Y., He, T., Song, G., Wu, F., Jiang, F., & Hu, J. (2013). One-pot morphology-controlled synthesis of various shaped mesoporous silica nanoparticles. *Journal of Materials Science, 48*, 5718–5726.

Henao, W., Jaramillo, L. Y., López, D., Romero-Sáez, M., & Buitrago-Sierra, R. (2020). Insights into the CO_2 capture over amine-functionalized mesoporous silica adsorbents derived from rice husk ash. *Journal of Environmental Chemical Engineering, 8*(5), 104362.

Jang, H. T., Park, Y., Ko, Y. S., Lee, J. Y., & Margandan, B. (2009). Highly siliceous MCM-48 from rice husk ash for CO_2 adsorption. *International Journal of Greenhouse Gas Control, 3*(5), 545–549.

Kishor, R., & Ghoshal, A. K. (2016). High molecular weight polyethyleneimine functionalized three dimensional mesoporous silica for regenerable CO_2 separation. *Chemical Engineering Journal, 300*, 236–244.

Kishor, R., & Ghoshal, A. K. (2017). Amine-modified mesoporous silica for CO_2 adsorption: The role of structural parameters. *Industrial and Engineering Chemistry Research, 56*(20), 6078–6087.

Krzyżak, A. T., Habina-Skrzyniarz, I., Machowski, G., & Mazur, W. (2020). Overcoming the barriers to the exploration of nanoporous shales porosity. *Microporous and Mesoporous Materials, 298*, 110003.

Kuila, U., & Prasad, M. (2013). Specific surface area and pore-size distribution in clays and shales. *Geophysical Prospecting, 61*(2), 341–362.

Lamb, W. F., Wiedmann, T., Pongratz, J., Andrew, R., Crippa, M., Olivier, J. G., Wiedenhofer, D., Mattioli, G., Khourdajie, A. A., House, J., Pachauri, S., Figueroa, M., Saheb, Y., Slade, R., Hubacek, K., Sun, L., Ribeiro, S. K., Khennas, S., Can, S. R., … Minx, J. (2021). A review of trends and drivers of greenhouse gas emissions by sector from 1990 to 2018. *Environmental Research Letters, 16*(7), 073005.

Li, H., Wang, S., Ling, F., & Li, J. (2006). Studies on MCM-48 supported cobalt catalyst for Fischer-Tropsch synthesis. *Journal of Molecular Catalysis a: Chemical, 244*(1–2), 33–40.

Li, Y., Tiwari, A. K., Ng, J. S., Seah, G. L., Lim, H. K., Suteewong, T., Tay, C. Y., Lam, Y. M., & Tan, K. W. (2022). One-Pot Synthesis of Aminated Bimodal Mesoporous Silica Nanoparticles as Silver-Embedded Antibacterial Nanocarriers and CO_2 Capture Sorbents. *ACS Applied Materials & Interfaces, 14*(46), 52279–52288.

Liao, P. Q., Chen, X. W., Liu, S. Y., Li, X. Y., Xu, Y. T., Tang, M., Rui, Z., Ji, H., Zhang, J. P., & Chen, X. M. (2016). Putting an ultrahigh concentration of amine groups into a metal–organic framework for CO_2 capture at low pressures. *Chemical Science, 7*(10), 6528–6533.

Liu, Y., Shi, J., Chen, J., Ye, Q., Pan, H., Shao, Z., & Shi, Y. (2010). Dynamic performance of CO_2 adsorption with tetraethylenepentamine-loaded KIT-6. *Microporous and Mesoporous Materials, 34*(1–3), 16–21.

Liu, F., Huang, K., Yoo, C. J., Okonkwo, C., Tao, D. J., Jones, C. W., & Dai, S. (2017a). Facilely synthesized meso-macroporous polymer as support of poly (ethyleneimine) for highly efficient and selective capture of CO_2. *Chemical Engineering Journal, 314*, 466–476.

Liu, Q., He, P., Qian, X., Fei, Z., Zhang, Z., Chen, X., & Shi, Y. (2017b). Enhanced CO_2 adsorption performance on hierarchical porous ZSM-5 zeolite. *Energy & Fuels, 31*(12), 13933–13941.

Liu, X., Zhou, K., Farndon, M., Meier, E., Stevens, L., Liu, H., & Sun, C. (2019). Mesocellular silica foam supported polyamine adsorbents for dry CO_2 scrubbing: Performance of single versus blended polyamines for impregnation. *Applied Energy, 255*, 113643.

Loganathan, S., Tikmani, M., & Ghoshal, A. K. (2013). Novel pore-expanded MCM-41 for CO_2 capture: Synthesis and characterization. *Langmuir, 29*(10), 3491–3499.

Lou, F., Zhang, A., Zhang, G., Ren, L., Guo, X., & Song, C. (2020). Enhanced kinetics for CO_2 sorption in amine-functionalized mesoporous silica nanosphere with inverted cone-shaped pore structure. *Applied Energy, 264*, 114637.

Malhis, A. A., Arar, S. H., Fayyad, M. K., & Hodali, H. A. (2018). Amino-and thiol-modified microporous silicalite-1 and mesoporous MCM-48 materials as potential effective adsorbents for Pb (II) in polluted aquatic systems. *Adsorption Science & Technology, 36*(1–2), 270–286.

Mamaghani, Z. G., Hawboldt, K. A., MacQuarrie, S., & Katz, M. J. (2024). Impact evaluation of coexisting gas CO on CO_2 adsorption on biochar derived from softwood shavings. *Separation and Purification Technology, 338*, 126529.

Mane, S., Gao, Z. Y., Li, Y. X., Liu, X. Q., & Sun, L. B. (2018). Rational fabrication of polyethylenimine-linked microbeads for selective CO_2 capture. *Industrial and Engineering Chemistry Research, 57*(1), 250–258.

Michalkiewicz, B., Majewska, J., Kądziołka, G., Bubacz, K., Mozia, S., & Morawski, A. W., (2014). Reduction of CO_2 by adsorption and reaction on surface of TiO_2-nitrogen modified photocatalyst. *Journal of CO_2 Utilization*, *5*, 47–52.

Mukherjee, S., & Samanta, A. N. (2022). Low to high-pressure CO_2 separation using amine-functionalized Mobile Composite Matter, isotherm modelling and heat of adsorption study. *Separation Science and Technology, 57*(2), 209–224.

Niu, M., Yang, H., Zhang, X., Wang, Y., & Tang, A. (2016). Amine-impregnated mesoporous silica nanotube as an

emerging nanocomposite for CO_2 capture. *ACS Applied Materials & Interfaces, 8*(27), 17312–17320.

Nwabueze, Q. A., & Leggett, S. (2024). Advancements in the Application of CO_2 Capture and Utilization Technologies-A Comprehensive Review. *Fuels, 5*(3), 508–532.

Pirouzmand, M., Amini, M. M., Safari, N., & Hamoule, T. (2013). Immobilization of cobalt phthalocyanine and tetrasulfophthalocyanine onto MCM-41 and MCM-48: Effect of immobilization method on catalytic activity. *Journal of the Brazilian Chemical Society, 24*, 1864–1870.

Qian, X., Yang, J., Fei, Z., Liu, Q., Zhang, Z., Chen, X., Tang, J., Cui, M., & Qiao, X. (2019). A simple strategy to improve PEI dispersion on MCM-48 with long-Alkyl chains template for efficient CO_2 adsorption. *Industrial and Engineering Chemistry Research, 58*(25), 10975–10983.

Rameli, N., Jumbri, K., Wahab, R. A., Ramli, A., & Huyop, F., (2018). Synthesis and characterization of mesoporous silica nanoparticles using ionic liquids as a template. *Journal of Physics: Conference Series*, *1123*(1), 012068. IOP Publishing.

Rashidi, N. A., Yusup, S., & Borhan, A. (2016). Isotherm and thermodynamic analysis of carbon dioxide on activated carbon. *Procedia Engineering, 148*, 630–637.

Ravutsov, M., Mitrev, Y., Shestakova, P., Lazarova, H., Simeonov, S., & Popova, M. (2021). CO_2 adsorption on modified mesoporous silicas: The role of the adsorption sites. *Nanomaterials, 11*(11), 2831.

Ren, J., Weng, H., Li, B., Chen, F., Liu, J., & Song, Z., (2022). The influence mechanism of pore structure of tectonically deformed coal on the adsorption and desorption hysteresis. In Pan, J., Ju, Y., Tan, J., Liu, S. (Eds.), Unconventional natural gas geoscience (pp. 125–140). Frontiers Media SA.

Sanz-Pérez, E. S., Arencibia, A., Sanz, R., & Calleja, G. (2016). New developments on carbon dioxide capture using amine-impregnated silicas. *Adsorption, 22*, 609–619.

Sanz-Pérez, E. S., Dantas, T. C. M., Arencibia, A., Calleja, G., Guedes, A. P. M. A., Araujo, A. S., & Sanz, R. (2017). Reuse and recycling of amine-functionalized silica materials for CO_2 adsorption. *Chemical Engineering Journal, 308*, 1021–1033.

Sanz-Pérez, E. S., Arencibia, A., Calleja, G., & Sanz, R. (2018). Tuning the textural properties of HMS mesoporous silica. Functionalization towards CO_2 adsorption. *Microporous and Mesoporous Materials, 260*, 235–244.

Sazegar, M. R., Dadvand, A., & Mahmoudi, A. (2017). Novel protonated Fe-containing mesoporous silica nanoparticle catalyst: Excellent performance cyclohexane oxidation. *RSC Advances, 7*(44), 27506–27514.

Schumacher, K., Ravikovitch, P. I., Du Chesne, A., Neimark, A. V., & Unger, K. K. (2000). Characterization of MCM-48 materials. *Langmuir, 16*(10), 4648–4654.

Shao, Y., Wang, L., Zhang, J., & Anpo, M. (2008). Synthesis and characterization of high hydrothermally stable Cr-MCM-48. *Microporous and Mesoporous Materials, 109*(1–3), 271–277.

Sing, K. S. W. (1982). Reporting physisorption data for gas/solid systems with special reference to the determination of surface area and porosity (Provisional). *Pure and Applied Chemistry, 54*(11), 2201–2218.

Singh, V. K., & Kumar, E. A. (2018). Comparative studies on CO_2 adsorption isotherms by solid adsorbents. *Materials Today Proceeding, 5*(11), 23033–23042.

Singh, J., Bhunia, H., & Basu, S. (2018). CO_2 adsorption on oxygen enriched porous carbon monoliths: Kinetics, isotherm and thermodynamic studies. *Journal of Industrial and Engineering Chemistry, 60*, 321–332.

Son, W. J., Choi, J. S., & Ahn, W. S. (2008). Adsorptive removal of carbon dioxide using polyethyleneimine-loaded mesoporous silica materials. *Microporous and Mesoporous Materials, 113*(1–3), 31–40.

Taba, P., Budi, P., & Puspitasari, A. Y., (2017). Adsorption of heavy metals on amine-functionalized MCM-48. *IOP Conference Series: Materials Science and Engineering*, *188*(1), 012015. IOP Publishing.

Taba, P., Mustafa, R. D. P., Ramang, L. M., & Kasim, A. H. (2018). Adsorption of Pb^{2+} on Thiol-functionalized Mesoporous Silica, SH-MCM-48. *Journal of Physics: Conference Series, 979*(1), 012058. IOP Publishing.

Tiwari, D., Goel, C., Bhunia, H., & Bajpai, P. K. (2017). Melamine-formaldehyde derived porous carbons for adsorption of CO_2 capture. *Journal of Environmental Management, 197*, 415–427.

Tiwari, D., Bhunia, H., & Bajpai, P. K. (2018). Adsorption of CO_2 on KOH activated, N-enriched carbon derived from urea formaldehyde resin: Kinetics, isotherm and thermodynamic studies. *Applied Surface Science, 439*, 760–771.

Vargas, D. P., Giraldo, L., & Moreno-Piraján, J. C. (2012). CO_2 adsorption on activated carbon honeycomb-monoliths: A comparison of Langmuir and Toth models. *International Journal of Molecular Sciences, 13*(7), 8388–8397.

Vazquez, N. I., Gonzalez, Z., Ferrari, B., & Castro, Y. (2017). Synthesis of mesoporous silica nanoparticles by sol–gel as nanocontainer for future drug delivery applications. *Boletín de la Sociedad Española de Cerámica y Vidrio, 56*(3), 139–145.

Venkatachalam, K., Visuvamithiran, P., Sundaravel, B., Palanichamy, M., & Murugesan, V. (2012). Catalytic performance of Al-MCM-48 molecular sieves for isopropylation of phenol with isopropyl acetate. *Chinese Journal of Catalysis, 33*(2–3), 478–486.

Vilarrasa-García, E., Cecilia, J. A., Santos, S. M. L., Cavalcante, C. L., Jr., Jiménez-Jiménez, J., Azevedo, D. C. S., & Rodríguez-Castellón, E. (2014). CO_2 adsorption on APTES functionalized mesocellular foams obtained from mesoporous silicas. *Microporous and Mesoporous Materials, 187*, 125–134.

Wang, J., Lu, J., Yang, J., Xiao, W., & Wang, J. (2012). Synthesis of ordered MCM-48 by introducing economical anionic surfactant as co-template. *Materials Letters, 78*, 199–201.

Wei, J., Shi, J., Pan, H., Su, Q., Zhu, J., & Shi, Y. (2009). Thermal and hydrothermal stability of amino-functionalized SBA-16 and promotion of hydrophobicity

by silylation. *Microporous and Mesoporous Materials, 117*(3), 596–602.

Xing, H. B., Pan, H. M., Fang, Y., Zhou, X. Y., Pan, Q. I. N., & Li, D. A. (2014). Construction of a tumor cell-targeting non-viral gene delivery vector with polyethylenimine modified with RGD sequence-containing peptide. *Oncology Letters, 7*(2), 487–492.

Xu, Y., Xiao, L., Chang, Y., Cao, Y., Chen, C., & Wang, D. (2020). pH and redox dual-responsive MSN-SS-CS as a drug delivery system in cancer therapy. *Materials., 13*(6), 1279.

Yan, X., Zhang, L., Zhang, Y., Qiao, K., Yan, Z., & Komarneni, S. (2011). Amine-modified mesocellular silica foams for CO_2 capture. *Chemical Engineering Journal, 168*(2), 918–924.

Yue, M. B., Chun, Y., Cao, Y., Dong, X., & Zhu, J. H. (2006). CO_2 capture by as-prepared SBA-15 with an occluded organic template. *Advanced Functional Materials, 16*(13), 1717–1722.

Zeleňák, V., Badaničová, M., Halamová, D., Čejka, J., Zukal, A., Murafa, N., & Goerigk, G. (2008). Amine-modified ordered mesoporous silica: Effect of pore size on carbon dioxide capture. *Chemical Engineering Journal, 144*(2), 336–342.

Zhang, L., Zhan, N., Jin, Q., Liu, H., & Hu, J. (2016). Impregnation of polyethylenimine in mesoporous multilamellar silica vesicles for CO_2 capture: A kinetic study. *Industrial and Engineering Chemistry Research, 55*(20), 5885–5891.

Zhang, G., Zhao, P., Hao, L., Xu, Y., & Cheng, H. (2019). A novel amine double functionalized adsorbent for carbon dioxide capture using original mesoporous silica molecular sieves as support. *Separation and Purification Technology, 209*, 516–527.

Zhao, Y., Zhu, Y., Zhu, T., Lin, G., Shao, M., Hong, W., & Hou, S. (2019). Polyethylenimine-based solid sorbents for CO_2 adsorption: Performance and secondary porosity. *Industrial and Engineering Chemistry Research, 58*(34), 15506–15515.